

# Higher Order Corrections to the Trilinear Higgs Self-Couplings in the Real NMSSM

Dao Thi Nhung, Margarete Mühlleitner, Juraj Streicher and Kathrin Walz

*Institut für Theoretische Physik, Karlsruher Institut für Technologie,  
76128 Karlsruhe, Germany*

## Abstract

After the discovery of a Higgs-like boson by the LHC experiments ATLAS and CMS, it is of crucial importance to determine its properties in order to not only identify it as the boson responsible for electroweak symmetry breaking but also to clarify the question if it is a Standard Model (SM) Higgs boson or the Higgs particle of some extension beyond the SM as *e.g.* supersymmetry. In this context, the precise prediction of the Higgs parameters as masses and couplings plays a crucial role for the proper distinction between different models. In extension of previous works on the loop-corrected Higgs boson masses of the Next-to-Minimal Supersymmetric Extension of the SM (NMSSM), we present here the calculation of the loop-corrected trilinear NMSSM Higgs self-couplings. The loop corrections turn out to have a substantial impact on the decay widths of Higgs-to-Higgs decays and on the production cross section of Higgs pairs via gluon fusion. They are therefore indispensable for the correct interpretation of the experimental Higgs results.

## 1 Introduction

In 2012 the Large Hadron Collider (LHC) experiments ATLAS and CMS announced the discovery of a new scalar particle [1, 2]. Since then experimental and theoretical activities have started to pin down the true nature of this particle. It has to be clarified if the particle is really the Higgs boson, *i.e.* the particle responsible for electroweak symmetry breaking (EWSB) without violating the gauge principles of the Standard Model (SM). And if so, whether it is the Higgs boson of the SM or one of an enlarged supersymmetric (SUSY) Higgs sector or some more exotic version of the Higgs particle, like *e.g.* a composite object. To this aim, the coupling strengths of the new particle to the other SM particles, its spin and CP-properties and finally its trilinear and quartic self-couplings have to be measured. While the absolute coupling values are not accessible at the LHC, fits can be performed to the measured signal strengths in the various Higgs search channels [3]. The Higgs spin and CP quantum numbers can be extracted from angular and threshold distributions in various Higgs production and decay channels [4]. The trilinear and quartic Higgs self-interactions finally are in principle accessible in double and triple Higgs production [5–9]. The knowledge of these couplings enables the reconstruction of the Higgs potential and allows to test if it has a non-vanishing vacuum expectation value (VEV) as required by the Higgs mechanism. This challenging experimental program necessitates on the theoretical side the precise prediction of production and decay cross sections in the model under consideration, in order to be able to interpret the experimental data correctly and to distinguish between different models. The cross sections have therefore to be evaluated including higher order corrections. However, not only these, but also the input parameters like masses and couplings have to be predicted with highest possible precision. It is well known *e.g.* that in the Minimal Supersymmetric extension of the SM (MSSM) the lightest Higgs boson mass is shifted beyond the theoretical tree-level bound of the  $Z$  boson mass only through the inclusion of higher-order corrections [10]. In this work we contribute to increasing the accuracy in the prediction of the Higgs parameters of the Next-to-Minimal Supersymmetric extension of the SM (NMSSM) [11–13]. We calculate the one-loop corrections to the trilinear Higgs self-couplings of the NMSSM Higgs bosons in the Feynman-diagrammatic approach, after having provided in previous works the one-loop corrections to the masses [14, 15].

The Higgs sector of the NMSSM consists of two complex Higgs doublets  $H_u$  and  $H_d$  and an additional complex singlet field  $S$ . The singlet field couples to the MSSM Higgs doublets through the interaction term  $\lambda S(H_u \epsilon H_d)$ . This allows for a dynamical solution of the  $\mu$  problem [16] when the neutral component of the singlet field acquires its VEV. Moreover, the NMSSM requires less fine-tuning than the MSSM in order to comply with the LHC discovery of a Higgs boson with mass around 125 GeV [17]. New contributions proportional to the quartic coupling increase the tree-level mass value of the lightest Higgs boson, so that compared to the MSSM less important radiative mass corrections are necessary to shift the tree-level mass value to the observed 125 GeV. This in turn allows for lighter stop masses and hence less fine-tuning. After EWSB we are left with seven Higgs bosons, which are in the CP-conserving NMSSM three neutral CP-even, two neutral CP-odd and two charged Higgs bosons. The enlarged Higgs sector leads to interesting phenomenological implications. Thus the SM-like Higgs boson, which is compatible with the LHC Higgs searches, can in general be either of the three neutral CP-even Higgs bosons. Most scenarios, however, which are in accordance with the experimental constraints, feature the lightest or the next-to-lightest

CP-even Higgs boson as the SM-like 125 GeV boson. Furthermore, the admixture of the singlet field can suppress the Higgs couplings to the other SM particles, so that light Higgs states may have escaped detection at Tevatron, LEP and LHC. The presence of light Higgs bosons entails possible new Higgs-to-Higgs decays such as *e.g.* the decay of a SM-like scalar Higgs boson into a pair of lighter pseudoscalars. From this discussion it becomes clear that the precise knowledge of the Higgs boson masses and couplings is inevitable to properly describe the Higgs phenomenology. It is needed to reanalyse and interpret correctly the LHC search results in the light of a possible NMSSM extension of the SM.

While in the MSSM the higher-order corrections to the Higgs boson masses have been calculated up to the inclusion of the leading contributions from three-loop order [10], the higher-order corrections to the NMSSM Higgs boson masses have not reached the same level of accuracy. For the CP conserving NMSSM the following corrections are available. In the effective potential approach the leading one-loop (s)top and (s)bottom contributions have been calculated [18]. The chargino, neutralino and scalar one-loop contributions are available at leading logarithmic accuracy [19]. The full one-loop contributions have been given in the  $\overline{\text{DR}}$  renormalisation scheme in Ref. [20,21], the  $\mathcal{O}(\alpha_t\alpha_s + \alpha_b\alpha_s)$  corrections in the approximation of zero external momentum in Ref. [20]. In addition, we have provided the full one-loop corrections in a mixed  $\overline{\text{DR}}$ -on-shell and in a pure on-shell renormalisation scheme [14]. As for the CP-violating NMSSM, CP-violating effects from the third generation squark sector, from the charged particle loops and from gauge boson contributions have been provided in the effective potential approach at one-loop level [22–24]. The full one-loop and logarithmically enhanced two-loop effects are available in the renormalisation group improved approach [25]. This has been complemented by the full one-loop corrections in the Feynman diagrammatic approach [15].

Both Higgs boson masses and Higgs self-interactions arise from the Higgs potential. They cannot be separated from each other. In order to consistently describe the Higgs sector including higher-order corrections, it is therefore not sufficient to only correct the Higgs boson masses. The trilinear and quartic Higgs self-interactions have to be evaluated at the same order in perturbation theory and within the same renormalisation scheme as the Higgs boson masses to allow for a consistent description of the Higgs boson phenomenology. While the phenomenology involving quartic Higgs self-couplings is most probably outside the reach of existing and future colliders, the trilinear Higgs self-couplings play a role in the determination of the Higgs boson branching ratios into SM particles, in the evaluation of Higgs-to-Higgs decays and in Higgs pair production processes. In this work we calculate the one-loop corrections to the trilinear Higgs self-couplings of the CP-conserving NMSSM in the Feynman-diagrammatic approach. We apply the mixed  $\overline{\text{DR}}$ -on-shell renormalisation scheme, which has been introduced in Ref. [14] for the one-loop corrections to the Higgs boson masses, and we study the phenomenological implications of these corrections.

The outline of our paper is as follows. In section 2 we briefly describe the loop corrections to the Higgs boson masses. We use this section to set up our notation, present details of the calculation of the Higgs mass corrections and introduce the renormalisation scheme. In contrast to our previous calculation [14] we also add leading two-loop contributions which have been taken over from Ref. [20]. Section 3 contains the calculation of the loop-corrected trilinear Higgs self-couplings. Section 4 is devoted to our numerical analysis. We first define in subsection 4.1 our input parameters and describe the constraints which we apply. In particular we seek a Higgs boson with

mass around 125 GeV that is compatible with the LHC results for the signal strengths in the various final states, while making sure that the remaining Higgs mass spectrum has not been excluded yet. In subsection 4.2 we discuss the effective trilinear Higgs couplings before we present in subsection 4.3 our results on Higgs-to-Higgs decays. Subsection 4.4 is devoted to the discussion of the effects of loop corrections to the trilinear Higgs self-couplings on Higgs pair production processes at the LHC. We conclude in section 5. In the Appendix A we list the tree-level trilinear Higgs couplings.

## 2 The loop-corrected Higgs boson masses

In this section we summarise the calculation of the loop corrections to the NMSSM Higgs boson masses. Since at one-loop order we apply the same procedure as in our previous publication [14] we repeat here only the main features for the purpose of setting up the notation and of introducing the renormalisation scheme. For details we refer the reader to Ref. [14].

We work in the framework of the NMSSM with a scale invariant superpotential. The Higgs mass matrix is derived from the corresponding NMSSM Higgs potential, which is obtained from the superpotential  $W_{NMSSM}$  of the NMSSM, the soft SUSY breaking terms and the  $D$ -term contributions. In terms of the Higgs doublet superfields  $\hat{H}_u$  and  $\hat{H}_d$ , which couple to the up- and down-type fermion superfields, respectively, and of the singlet superfield  $\hat{S}$ , the superpotential is given by

$$W_{NMSSM} = W_{MSSM} - \epsilon_{ij} \lambda \hat{S} \hat{H}_d^i \hat{H}_u^j + \frac{1}{3} \kappa \hat{S}^3. \quad (1)$$

The indices of the  $SU(2)_L$  fundamental representation are denoted by  $i, j = 1, 2$ , and  $\epsilon_{ij}$  is the totally antisymmetric tensor with  $\epsilon_{12} = \epsilon^{12} = 1$ . The dimensionless parameters  $\lambda$  and  $\kappa$  are taken to be real as we assume CP conservation. The MSSM superpotential  $W_{MSSM}$  reads in terms of the quark and lepton superfields and their charge conjugate (denoted by the superscript  $c$ ),  $\hat{Q}, \hat{U}^c, \hat{D}^c, \hat{L}, \hat{E}^c$ ,

$$W_{MSSM} = \epsilon_{ij} [y_e \hat{H}_d^i \hat{L}^j \hat{E}^c + y_d \hat{H}_d^i \hat{Q}^j \hat{D}^c - y_u \hat{H}_u^i \hat{Q}^j \hat{U}^c]. \quad (2)$$

For simplicity colour and generation indices have been suppressed. Following common NMSSM constructions we have assumed the MSSM  $\mu$  term to be zero and also terms linear and quadratic in  $\hat{S}$ . The NMSSM soft SUSY breaking Lagrangian expressed in terms of the component fields  $H_u, H_d$  and  $S$  reads

$$\mathcal{L}_{soft} = \mathcal{L}_{soft, MSSM} - m_S^2 |S|^2 + (\epsilon_{ij} \lambda A_\lambda S H_d^i H_u^j - \frac{1}{3} \kappa A_\kappa S^3 + h.c.). \quad (3)$$

It contains the soft SUSY breaking MSSM contribution

$$\begin{aligned} \mathcal{L}_{soft, MSSM} = & -m_{H_d}^2 H_d^\dagger H_d - m_{H_u}^2 H_u^\dagger H_u - m_Q^2 \tilde{Q}^\dagger \tilde{Q} - m_L^2 \tilde{L}^\dagger \tilde{L} - m_U^2 \tilde{u}_R^* \tilde{u}_R - m_D^2 \tilde{d}_R^* \tilde{d}_R \\ & - m_E^2 \tilde{e}_R^* \tilde{e}_R - (\epsilon_{ij} [y_e A_e H_d^i \tilde{L}^j \tilde{e}_R^* + y_d A_d H_d^i \tilde{Q}^j \tilde{d}_R^* - y_u A_u H_u^i \tilde{Q}^j \tilde{u}_R^*] + h.c.) \\ & - \frac{1}{2} (M_1 \tilde{B} \tilde{B} + M_2 \tilde{W}_k \tilde{W}_k + M_3 \tilde{G} \tilde{G} + h.c.), \end{aligned} \quad (4)$$

where  $\tilde{Q} = (\tilde{u}_L, \tilde{d}_L)^T$  and  $\tilde{L} = (\tilde{\nu}_L, \tilde{e}_L)^T$  with tilde denoting the scalar components of the corresponding quark and lepton superfields. The soft SUSY breaking gaugino mass terms for the gaugino fields  $\tilde{B}, \tilde{W}_k$  ( $k = 1, 2, 3$ ) and  $\tilde{G}$  are summarised in the last line of Eq. (4) (the summation

over paired indices is implicit). Working in the CP-invariant NMSSM the soft SUSY breaking trilinear couplings  $A_x$  ( $x = \lambda, \kappa, d, u, e$ ) and gaugino mass parameters  $M_k$  are taken to be real. Furthermore, squark and slepton mixing between the generations is neglected. Like in the majority of phenomenological NMSSM constructions we have omitted possible soft SUSY breaking terms linear and quadratic in the singlet field  $S$ . After electroweak symmetry breaking the neutral components of the Higgs doublet and singlet fields acquire non-vanishing vacuum expectation values. Substituting the expansions of the Higgs fields about their VEVs  $v_u, v_d$  and  $v_s$ , which are chosen to be real and positive,

$$H_d = \begin{pmatrix} (v_d + h_d + ia_d)/\sqrt{2} \\ h_d^- \end{pmatrix}, \quad H_u = \begin{pmatrix} h_u^+ \\ (v_u + h_u + ia_u)/\sqrt{2} \end{pmatrix}, \quad S = \frac{v_s + h_s + ia_s}{\sqrt{2}}, \quad (5)$$

into the Higgs potential  $V_H$ , which expressed in terms of the Higgs component fields reads,

$$\begin{aligned} V_H = & (|\lambda S|^2 + m_{H_d}^2)H_{d,i}^*H_{d,i} + (|\lambda S|^2 + m_{H_u}^2)H_{u,i}^*H_{u,i} + m_S^2|S|^2 \\ & + \frac{1}{8}(g_2^2 + g_1^2)(H_{d,i}^*H_{d,i} - H_{u,i}^*H_{u,i})^2 + \frac{1}{2}g_2^2|H_{d,i}^*H_{u,i}|^2 \\ & + |-\epsilon^{ij}\lambda H_{d,i}H_{u,j} + \kappa S^2|^2 + [-\epsilon^{ij}\lambda A_\lambda SH_{d,i}H_{u,j} + \frac{1}{3}\kappa A_\kappa S^3 + \text{h.c.}], \end{aligned} \quad (6)$$

we have

$$\begin{aligned} V_H = & V_H^{\text{const}} + t_{h_d}h_d + t_{h_u}h_u + t_{h_s}h_s + \frac{1}{2}(h_d, h_u, h_s) M_S^2 \begin{pmatrix} h_d \\ h_u \\ h_s \end{pmatrix} + \frac{1}{2}(a_d, a_u, a_s) M_a^2 \begin{pmatrix} a_d \\ a_u \\ a_s \end{pmatrix} \\ & + (h_d^-, h_u^-) M_C^2 \begin{pmatrix} h_d^+ \\ h_u^+ \end{pmatrix} + \lambda_{ijk}^{hhh} h_i h_j h_k + \lambda_{ijk}^{haa} h_i a_j a_k + V_H^{4\phi}, \end{aligned} \quad (7)$$

with  $i, j, k = d, u, s$ . Equation (7) contains the tadpole coefficients  $t_{h_i}$  of the terms linear in the Higgs fields  $h_i$ , the mass matrices squared and the trilinear Higgs self-interactions. The constant terms are summarised in  $V_H^{\text{const}}$  and the quartic Higgs interactions in  $V_H^{4\phi}$ . They are not specified here as they are not needed for our calculation. The  $3 \times 3$  mass matrices squared for the neutral CP-even and CP-odd Higgs sector, respectively, are denoted by  $M_S^2$  and  $M_a^2$ , the  $2 \times 2$  charged Higgs mass matrix squared by  $M_C^2$  and the trilinear Higgs self-couplings by  $\lambda_{ijk}^{\phi\phi'\phi''}$ . Explicit expressions for the couplings are given in Appendix A. Performing a first rotation of the CP-odd fields  $(a_d, a_u, a_s)$ ,

$$\begin{pmatrix} a \\ a_s \\ G \end{pmatrix} = \mathcal{R}_G \begin{pmatrix} a_d \\ a_u \\ a_s \end{pmatrix} \equiv \begin{pmatrix} s_{\beta_n} & c_{\beta_n} & 0 \\ 0 & 0 & 1 \\ c_{\beta_n} & -s_{\beta_n} & 0 \end{pmatrix} \begin{pmatrix} a_d \\ a_u \\ a_s \end{pmatrix}, \quad (8)$$

allows to separate a massless Goldstone boson  $G$  and yields the pseudoscalar mass matrix squared

$$M_P^2 = \mathcal{R}^G M_a^2 (\mathcal{R}^G)^T. \quad (9)$$

Here and in the following we adopt the shorthand notation  $c_x \equiv \cos x$ ,  $s_x \equiv \sin x$ . At tree-level the angle  $\beta_n$  coincides with the angle  $\beta$  defined by the ratio of the two VEVs  $v_u$  and  $v_d$ ,  $\tan \beta = v_u/v_d$ .

Explicit expressions for the scalar and pseudoscalar mass matrices squared  $M_S^2$  and  $M_P^2$  as well as for the tadpole parameters can be found in [14], and for the charged Higgs mass matrix  $M_C$  in [15]. The CP-even Higgs mass eigenstates  $h_m$  ( $m = 1, 2, 3$ ) are obtained via the diagonalisation of the mass mixing matrix squared  $M_S^2$  by an orthogonal transformation,

$$\begin{pmatrix} h_1, h_2, h_3 \end{pmatrix}^T = (\mathcal{R}^S) \begin{pmatrix} h_d, h_u, h_s \end{pmatrix}^T, \quad \text{diag}(m_{h_1}^2, m_{h_2}^2, m_{h_3}^2) = \mathcal{R}^S M_S^2 (\mathcal{R}^S)^T. \quad (10)$$

The mass eigenstates are ordered by ascending mass with  $m_{h_1} \leq m_{h_2} \leq m_{h_3}$ . The CP-odd mass eigenstates  $a_i \equiv a_1, a_2, G$  ( $i = 1, 2, 3$ ) are obtained via an orthogonal rotation  $\mathcal{R}^P$  applied to  $h^P = (a, a_s, G)^T$ ,

$$a_i = \mathcal{R}_{ij}^P h_j^P \quad i, j = 1, 2, 3, \quad (11)$$

yielding the diagonal mass matrix squared

$$\text{diag}(m_{a_1}^2, m_{a_2}^2, 0) = \mathcal{R}^P M_P^2 (\mathcal{R}^P)^T = \mathcal{R}^P \mathcal{R}^G M_a^2 (\mathcal{R}^P \mathcal{R}^G)^T. \quad (12)$$

Note that at tree-level  $\mathcal{R}_{33}^P = 1$  and  $\mathcal{R}_{3i}^P = \mathcal{R}_{i3}^P = 0$  for  $i \neq 3$ .

At lowest order, the Higgs potential is determined by a set of twelve parameters consisting of the electroweak gauge couplings  $g_1$  and  $g_2$ , the three VEVs, the soft SUSY breaking mass parameters of the doublet and singlet Higgs fields and the new NMSSM related parameters and soft SUSY breaking couplings, hence

$$g_1, g_2, v_d, v_u, v_s, m_{H_d}^2, m_{H_u}^2, m_S^2, \lambda, \kappa, A_\lambda, A_\kappa. \quad (13)$$

For physical interpretations it is convenient to replace some of these parameters. Thus the minimisation conditions of the Higgs potential  $V$  can be exploited to trade  $m_{H_d}^2, m_{H_u}^2$  and  $m_S^2$  for the tadpole parameters  $t_{h_d}, t_{h_u}$  and  $t_{h_s}$ . The charged Higgs boson mass  $M_{H^\pm}$  is used instead of the soft SUSY breaking coupling  $A_\lambda$  and the parameters  $g_1, g_2, v_u$  and  $v_d$  are replaced by the gauge boson masses  $M_W$  and  $M_Z$ , the electric charge  $e$  and  $\tan \beta$ . We are then left with the 'physical' parameter set

$$M_Z, M_W, M_{H^\pm}, t_{h_d}, t_{h_u}, t_{h_s}, e, \tan \beta, \lambda, v_s, \kappa, A_\kappa. \quad (14)$$

The tree-level relations between the two parameter sets of Eq. (13) and Eq. (14) can be found in [14]. Note that although the three tadpole parameters vanish at the stable minimum of the potential, they have been kept for the purpose of renormalisation at loop level. The terms linear in the Higgs fields get loop contributions at higher order, and the tadpole parameters are renormalised such that the conditions of a stable minimum are fulfilled by the Higgs potential.

The calculation of the loop corrections to the Higgs boson masses and decays leads to ultraviolet divergences which can be absorbed by the renormalisation of the parameters entering the loop calculation. We choose here the mixed renormalisation scheme proposed in [14]. In this scheme part of the parameters are renormalised in the on-shell (OS) scheme, the remaining ones via  $\overline{\text{DR}}$  conditions. We slightly abuse the term on-shell condition as we apply it also for the renormalisation conditions of the tadpole parameters. In detail we have,

$$\underbrace{M_Z, M_W, M_{H^\pm}, t_{h_u}, t_{h_d}, t_{h_s}, e}_{\text{on-shell scheme}}, \underbrace{\tan \beta, \lambda, v_s, \kappa, A_\kappa}_{\overline{\text{DR}} \text{ scheme}}. \quad (15)$$

The corresponding counterterms are given explicitly in Ref. [14]. The only difference consists in the electric charge  $e$  where we use the fine structure constant at the  $Z$  boson mass  $M_Z$ ,  $\alpha = \alpha(M_Z)$ , as an input in order to make the results independent of  $\ln m_f$  from the light fermions,  $f \neq t$ . The counterterm  $\delta Z_e$  of  $e$  is therefore modified as [26]

$$\begin{aligned}\delta Z_e^{\alpha(M_Z)} &= \delta Z_e^{\alpha(0)} - \frac{1}{2} \Delta \alpha(M_Z^2), \\ \Delta \alpha(M_Z^2) &= \left. \frac{\partial \Sigma_T^{AA}}{\partial k^2} \right|_{k^2=0} - \frac{\text{Re} \Sigma_T^{AA}(M_Z^2)}{M_Z^2},\end{aligned}\quad (16)$$

where the transverse part of the photon self-energy  $\Sigma_T^{AA}$  includes only the light fermion contributions. For the Higgs field wave functions we also use the  $\overline{\text{DR}}$  scheme.

The loop-corrected Higgs masses squared are determined numerically. They are given as the zeros of the determinant of the two-point vertex functions for the scalars,  $\hat{\Gamma}^S(p^2)$ , and the pseudoscalars,  $\hat{\Gamma}^P(p^2)$ , respectively. For the scalar bosons it reads

$$\begin{aligned}\hat{\Gamma}^S(p^2) &= i(p^2 - \hat{M}_S^2(p^2)) \\ &= i \begin{pmatrix} p^2 - m_{h_1}^2 + \hat{\Sigma}_{h_1 h_1}(p^2) & \hat{\Sigma}_{h_1 h_2}(p^2) & \hat{\Sigma}_{h_1 h_3}(p^2) \\ \hat{\Sigma}_{h_2 h_1}(p^2) & p^2 - m_{h_2}^2 + \hat{\Sigma}_{h_2 h_2}(p^2) & \hat{\Sigma}_{h_2 h_3}(p^2) \\ \hat{\Sigma}_{h_3 h_1}(p^2) & \hat{\Sigma}_{h_3 h_2}(p^2) & p^2 - m_{h_3}^2 + \hat{\Sigma}_{h_3 h_3}(p^2) \end{pmatrix}\end{aligned}\quad (17)$$

and for the pseudoscalar Higgs bosons

$$\hat{\Gamma}^P(p^2) = i(p^2 - \hat{M}_A^2(p^2)) = i \begin{pmatrix} p^2 - m_{a_1}^2 + \hat{\Sigma}_{a_1 a_1}(p^2) & \hat{\Sigma}_{a_1 a_2}(p^2) \\ \hat{\Sigma}_{a_2 a_1}(p^2) & p^2 - m_{a_2}^2 + \hat{\Sigma}_{a_2 a_2}(p^2) \end{pmatrix}.\quad (18)$$

By  $\hat{\Sigma}$  we denote the renormalised self-energy built from the unrenormalised self-energy and tadpole contributions evaluated at one-loop order and the counterterms in the mixed renormalisation scheme. They are functions of the external momentum squared  $p^2$ . We furthermore included two-loop corrections, as will be explained below. The masses squared  $m_{h_i}^2, m_{a_l}^2$  ( $i = 1, 2, 3, l = 1, 2$ ) are taken at tree-level as indicated by the small letter  $m$  for the mass. Note that we have not taken into account the mixing of the pseudoscalars  $a_1$  and  $a_2$  with the Goldstone boson  $G$  and the longitudinal component of the  $Z$  boson, as we have checked explicitly that this mixing gives negligible contributions to the one-loop corrected Higgs boson masses. However, the mixing is taken into account in the computation of the loop corrections to the Higgs boson decays into two lighter Higgs bosons. The mass eigenvalues are obtained in an iterative procedure. For example, in order to get the lightest CP-even Higgs mass, in the first step the external momentum squared  $p^2$  is set equal to the  $h_1$  tree-level mass. The mass matrix squared is then diagonalised and the thus obtained lightest mass eigenvalue is reinserted into the self-energies, to calculate the mass eigenvalue in the next iteration. This procedure is repeated until the difference in the mass eigenvalue of two subsequent iterations is less than  $10^{-10}$  GeV. The eigenvalues are in general complex, and the loop corrected Higgs boson masses are given by the real part. They are sorted by ascending mass, as

$$M_{H_1}^2 < M_{H_2}^2 < M_{H_3}^2 \quad \text{and} \quad M_{A_1}^2 < M_{A_2}^2.\quad (19)$$

We denote the loop-corrected masses by capital letters,  $M_{H_i}, M_{A_l}$  ( $i = 1, 2, 3, l = 1, 2$ ) contrary to

the tree-level masses with small letters.

As indicated above, in order to improve the loop-corrected Higgs boson masses, we have included in the mass matrices  $\hat{M}_S^2(p^2)$  and  $\hat{M}_P^2(p^2)$  the known two-loop  $\mathcal{O}(\alpha_s\alpha_t + \alpha_s\alpha_b)$  corrections [20], which have been evaluated in the limit of zero external momentum. In this calculation the  $\overline{\text{DR}}$  renormalisation scheme has been applied in the (s)top and (s)bottom sectors. Therefore, in order to use these corrections consistently, we use the running  $\overline{\text{DR}}$  top and bottom quark masses in the evaluation of the one-loop renormalised self-energies. Using as input the top quark pole mass  $M_t$ , we first translate it to the running  $\overline{\text{MS}}$  top mass  $m_t^{\overline{\text{MS}}}(M_t)$  by applying the two-loop relation, see *e.g.* [27] and references therein,

$$m_t^{\overline{\text{MS}}}(M_t) = \left( 1 - \frac{4}{3} \left( \frac{\alpha_s(M_t)}{\pi} \right) - 9.1253 \left( \frac{\alpha_s(M_t)}{\pi} \right)^2 \right) M_t, \quad (20)$$

where  $\alpha_s$  is the strong coupling constant evaluated at two-loop order. As for the bottom quark mass input, it is already given as an  $\overline{\text{MS}}$  mass at the scale  $m_b^{\overline{\text{MS}}}$ . Both  $m_t^{\overline{\text{MS}}}(M_t)$  and  $m_b^{\overline{\text{MS}}}(m_b^{\overline{\text{MS}}})$  are then evolved up to the renormalisation scale  $\mu_R$ , by using the two-loop formula

$$m_t^{\overline{\text{MS}}}(\mu_R) = U_6(\mu_R, M_t) m_t^{\overline{\text{MS}}}(M_t) \quad \text{for } \mu_R > M_t, \quad (21)$$

$$m_b^{\overline{\text{MS}}}(\mu_R) = \begin{cases} U_6(\mu_R, M_t) U_5(M_t, m_b^{\overline{\text{MS}}}) m_b^{\overline{\text{MS}}}(m_b^{\overline{\text{MS}}}) & \text{for } \mu_R > M_t, \\ U_5(\mu_R, m_b^{\overline{\text{MS}}}) m_b^{\overline{\text{MS}}}(m_b^{\overline{\text{MS}}}) & \text{for } \mu_R \leq M_t, \end{cases} \quad (22)$$

where the evolution factor  $U_n$  reads (see *e.g.* [28])

$$U_n(Q_2, Q_1) = \left( \frac{\alpha_s(Q_2)}{\alpha_s(Q_1)} \right)^{d_n} \left[ 1 + \frac{\alpha_s(Q_1) - \alpha_s(Q_2)}{4\pi} J_n \right], \quad Q_2 > Q_1$$

$$d_n = \frac{12}{33 - 2n}, \quad J_n = -\frac{8982 - 504n + 40n^2}{3(33 - 2n)^2}, \quad (23)$$

with  $n$  being the number of active quark flavors ( $n = 5$  for  $m_b^{\overline{\text{MS}}}(m_b^{\overline{\text{MS}}}) < Q \leq M_t$  and  $n = 6$  for  $Q > M_t$ ). From the  $\overline{\text{MS}}$  masses the  $\overline{\text{DR}}$  masses are computed by using the two-loop relation [29],

$$m_{t/b}^{\overline{\text{DR}}}(\mu_R) = m_{t/b}^{\overline{\text{MS}}}(\mu_R) \left[ 1 - \frac{\alpha_s(\mu_R)}{3\pi} - \frac{\alpha_s^2(\mu_R)}{144\pi^2} (73 - 3n) \right]. \quad (24)$$

In addition, the possibly large supersymmetric corrections are resummed into the effective top and bottom quark masses [28, 30–32],

$$m_t^{\text{eff}} = \frac{m_t^{\overline{\text{DR}}}(\mu_R)}{1 + \delta m_t + \Delta m_t / \tan \beta} \quad \text{and} \quad m_b^{\text{eff}} = \frac{m_b^{\overline{\text{DR}}}(\mu_R)}{1 + \delta m_b + \Delta m_b \tan \beta}, \quad (25)$$

where

$$\Delta m_t = \frac{2\alpha_s(\mu_R)}{3\pi} m_{\tilde{g}} \mu_{\text{eff}} I(m_{\tilde{t}_1}^2, m_{\tilde{t}_2}^2, m_{\tilde{g}}^2) + \frac{y_b^2}{16\pi^2} A_b \mu_{\text{eff}} I(m_{\tilde{b}_1}^2, m_{\tilde{b}_2}^2, \mu_{\text{eff}}^2), \quad (26)$$

$$\Delta m_b = \frac{2\alpha_s(\mu_R)}{3\pi} m_{\tilde{g}} \mu_{\text{eff}} I(m_{\tilde{b}_1}^2, m_{\tilde{b}_2}^2, m_{\tilde{g}}^2) + \frac{y_t^2}{16\pi^2} A_t \mu_{\text{eff}} I(m_{\tilde{t}_1}^2, m_{\tilde{t}_2}^2, \mu_{\text{eff}}^2), \quad (27)$$

$$\delta m_t = -\frac{2\alpha_s(\mu_R)}{3\pi} m_{\tilde{g}} A_t I(m_{\tilde{t}_1}^2, m_{\tilde{t}_2}^2, m_{\tilde{g}}^2) - \frac{y_b^2}{16\pi^2} \mu_{\text{eff}}^2 I(m_{\tilde{b}_1}^2, m_{\tilde{b}_2}^2, \mu_{\text{eff}}^2), \quad (28)$$

$$\delta m_b = -\frac{2\alpha_s(\mu_R)}{3\pi} m_{\tilde{g}} A_b I(m_{\tilde{b}_1}^2, m_{\tilde{b}_2}^2, m_{\tilde{g}}^2) - \frac{y_t^2}{16\pi^2} \mu_{\text{eff}}^2 I(m_{\tilde{t}_1}^2, m_{\tilde{t}_2}^2, \mu_{\text{eff}}^2), \quad (29)$$



with the effective  $\mu$ -parameter  $\mu_{\text{eff}} \equiv \lambda v_s/\sqrt{2}$ , the Yukawa couplings  $y_t \equiv \sqrt{2}m_t^{\overline{\text{DR}}}(\mu_R)/v_u$  and  $y_b \equiv \sqrt{2}m_b^{\overline{\text{DR}}}(\mu_R)/v_d$  and with the auxiliary function

$$I(a, b, c) = -\frac{ab \ln(a/b) + bc \ln(b/c) + ca \ln(c/a)}{(a-b)(b-c)(c-a)}. \quad (30)$$

### 3 Loop-Corrected Higgs-to-Higgs Decays

In this section we present the calculation of the loop-corrected partial decay widths of all kinematically allowed Higgs boson decays into two lighter Higgs bosons,  $H_i \rightarrow H_j H_k$ ,  $H_i \rightarrow A_l A_m$  and  $A_l \rightarrow A_m H_i$  ( $i, j, k = 1, 2, 3$ ,  $l, m = 1, 2$ ). The two-body decay width of a scalar  $a$  decaying into two scalars  $b$  and  $c$  is given by

$$\Gamma(a \rightarrow bc) = R \frac{\lambda^{1/2}(m_a^2, m_b^2, m_c^2)}{16\pi m_a^3} |\mathcal{M}_{a \rightarrow bc}|^2, \quad (31)$$

where  $R = 1/2!$  for two identical final state particles and  $R = 1$  otherwise. The decay amplitude is denoted by  $\mathcal{M}_{a \rightarrow bc}$  and

$$\lambda(x, y, z) = x^2 + y^2 + z^2 - 2xy - 2xz - 2yz. \quad (32)$$

In order to calculate the decay amplitude at one-loop order, one has to take into account that not only the masses of the Higgs bosons receive corrections, but also the fields themselves are affected. In the  $\overline{\text{DR}}$  scheme, which we are using for the Higgs field renormalisation, the residue of the Higgs boson propagators is not equal to one so that finite wave-function renormalisation factors  $\mathbf{Z}$  have to be taken into account in order to ensure the on-shell properties of external Higgs bosons [33, 34]. The transformation of the interaction states  $h_u, h_d, h_s$  and  $a, a_s$ , respectively, to the loop-corrected mass eigenstates, which we denote by capital letters,  $H_1, H_2, H_3$  and  $A_1, A_2$ , is then performed by radiatively corrected transformation matrices for the scalar and pseudoscalar sector,  $\mathcal{R}^{S,l}$ ,  $\mathcal{R}^{P,l}$ , which are given by

$$\mathcal{R}_{is}^{S,l} = (\mathbf{Z}^S)_{ij} \mathcal{R}_{js}^S, \quad i, j, s = 1, 2, 3, \quad (33)$$

$$\mathcal{R}_{is}^{P,l} = (\mathbf{Z}^P)_{ij} \mathcal{R}_{js}^P, \quad i, j, s = 1, 2. \quad (34)$$

They are built up by the finite scalar and pseudoscalar wave-function renormalisation factors,  $\mathbf{Z}^S$  and  $\mathbf{Z}^P$ , and by the respective rotation matrix  $\mathcal{R}^S$ ,  $\mathcal{R}^P$ , performing the rotation from the interaction states to the mass eigenstates at tree-level, as defined in Eq. (10) and Eq. (11). Hence, for the scalar case, the indices correspond in ascending order to the following Higgs entries:  $i \hat{=} H_1, H_2, H_3$ ,  $j \hat{=} h_1, h_2, h_3$ ,  $s \hat{=} h_d, h_u, h_s$ . And for the pseudoscalar case:  $i \hat{=} A_1, A_2$ ,  $j \hat{=} a_1, a_2$ ,  $s \hat{=} a, a_s$ . The wave-function renormalisation factor matrices are given by [35]

$$\mathbf{Z}^S = \begin{pmatrix} \sqrt{\hat{Z}_{H_1}} & \sqrt{\hat{Z}_{H_1}} \hat{Z}_{H_1 H_2} & \sqrt{\hat{Z}_{H_1}} \hat{Z}_{H_1 H_3} \\ \sqrt{\hat{Z}_{H_2}} \hat{Z}_{H_2 H_1} & \sqrt{\hat{Z}_{H_2}} & \sqrt{\hat{Z}_{H_2}} \hat{Z}_{H_2 H_3} \\ \sqrt{\hat{Z}_{H_3}} \hat{Z}_{H_3 H_1} & \sqrt{\hat{Z}_{H_3}} \hat{Z}_{H_3 H_2} & \sqrt{\hat{Z}_{H_3}} \end{pmatrix}, \quad (35)$$

for the scalar Higgs bosons and by

$$\mathbf{Z}^P = \begin{pmatrix} \sqrt{\hat{Z}_{A_1}} & \sqrt{\hat{Z}_{A_1}} \hat{Z}_{A_1 A_2} \\ \sqrt{\hat{Z}_{A_2}} \hat{Z}_{A_2 A_1} & \sqrt{\hat{Z}_{A_2}} \end{pmatrix}, \quad (36)$$

for the pseudoscalar sector, with

$$\hat{Z}_i = \frac{1}{\left(\frac{i}{\Delta_{ii}(p^2)}\right)'(M_i^2)} \quad \text{and} \quad \hat{Z}_{ij} = \frac{\Delta_{ij}(p^2)}{\Delta_{ii}(p^2)} \Big|_{p^2=M_i^2} \quad (37)$$

for CP-even Higgs bosons  $i, j = H_1, H_2, H_3$  and for CP-odd Higgs bosons  $i, j = A_1, A_2$ . The diagonal  $\Delta_{ii}$  and the off-diagonal  $\Delta_{ij}$  are given by the matrix elements of the two-point vertex function matrices for the scalars,  $\hat{\Gamma}^S$ , Eq. (17), and the pseudoscalars,  $\hat{\Gamma}^P$ , Eq. (18), as

$$\Delta^S = - \left[ \hat{\Gamma}^S(p^2) \right]^{-1}, \quad \Delta^P = - \left[ \hat{\Gamma}^P(p^2) \right]^{-1}. \quad (38)$$

The prime in Eq. (37) denotes the derivative with respect to  $p^2$ . Note also that at one-loop order the complex eigenvalues of the loop-corrected two-point vertex functions are used in the evaluation of the wave function renormalisation factors, *i.e.*  $M_i$  in Eq. (37) includes also imaginary parts. The mixing matrix elements in this approach therefore include the full momentum dependence and imaginary parts of the one-loop Higgs boson self-energies. The evaluation of the wave function renormalisation factors at zero external momentum,  $p^2 = 0$ , which correspond to the result in the effective potential approximation, on the other hand leads to a unitary mixing matrix.

With these definitions, the amplitudes of Higgs boson decays at higher order can then be written as follows ( $i, j, k = 1, 2, 3, l, m = 1, 2$ )

$$\mathcal{M}_{H_i \rightarrow H_j H_k} = \sum_{i', j', k'=1}^3 \mathbf{z}_{ii'}^S \mathbf{z}_{jj'}^S \mathbf{z}_{kk'}^S (\lambda_{h_{i'} h_{j'} h_{k'}} + \delta M_{h_{i'} h_{j'} h_{k'}}^{1\text{PI}}), \quad (39)$$

$$\mathcal{M}_{H_i \rightarrow A_l A_m} = \sum_{i'=1}^3 \sum_{l', m'=1}^2 \mathbf{z}_{ii'}^S \mathbf{z}_{ll'}^P \mathbf{z}_{mm'}^P (\lambda_{h_{i'} a_{l'} a_{m'}} + \delta M_{h_{i'} a_{l'} a_{m'}}^{1\text{PI}}) + \delta M_{H_i \rightarrow A_l A_m}^{G, \text{Zmix}}, \quad (40)$$

$$\mathcal{M}_{A_l \rightarrow A_m H_i} = \sum_{i'=1}^3 \sum_{l', m'=1}^2 \mathbf{z}_{ii'}^S \mathbf{z}_{ll'}^P \mathbf{z}_{mm'}^P (\lambda_{h_{i'} a_{l'} a_{m'}} + \delta M_{a_{l'} a_{m'} h_{i'}}^{1\text{PI}}) + \delta M_{A_l \rightarrow A_m H_i}^{G, \text{Zmix}}, \quad (41)$$

where  $\lambda_{h_{i'} h_{j'} h_{k'}}$ ,  $\lambda_{h_{i'} a_{l'} a_{m'}}$  are the trilinear Higgs couplings at tree-level. Their explicit expressions are given in Appendix A. The 1-point irreducible (1PI) contributions to the vertex functions are denoted by  $\delta M_{abc}^{1\text{PI}}$ . Generic diagrams are shown in Fig. 1. They are built up by two- and three-point functions. The two-point functions involve four-point vertices between two Higgs bosons and two scalars (Goldstone bosons, Higgs bosons, sleptons, squarks, sneutrinos) as well as four point vertices between two Higgs bosons and two gauge bosons ( $Z$  or  $W^\pm$ ), see first row of Fig. 1. The three-point functions are given by loops over scalars, gauge bosons, fermions as well as ghost particles ( $\eta = \eta_Z, \eta_{W^\pm}$ ), see second and third row of Fig. 1. In addition to these diagrams the counterterms to the tree-level Higgs couplings are included in  $\delta M^{1\text{PI}}$ .

The  $\delta M_{a \rightarrow bc}^{G, \text{Zmix}}$  stands for the sum of the contributions from the mixing of the CP-odd Higgs boson with the Goldstone ( $G$ ) boson and with the  $Z$  boson, respectively. We use tree-level masses for the Higgs bosons in the loops in order to ensure the proper cancellation of the UV-divergent pieces. But we use the loop-corrected Higgs boson masses for the external particles in the evaluation of the wave-function renormalisation factors, amplitudes and decay widths. While this does not affect the UV-finite property of these quantities, the use of the loop-corrected Higgs boson masses

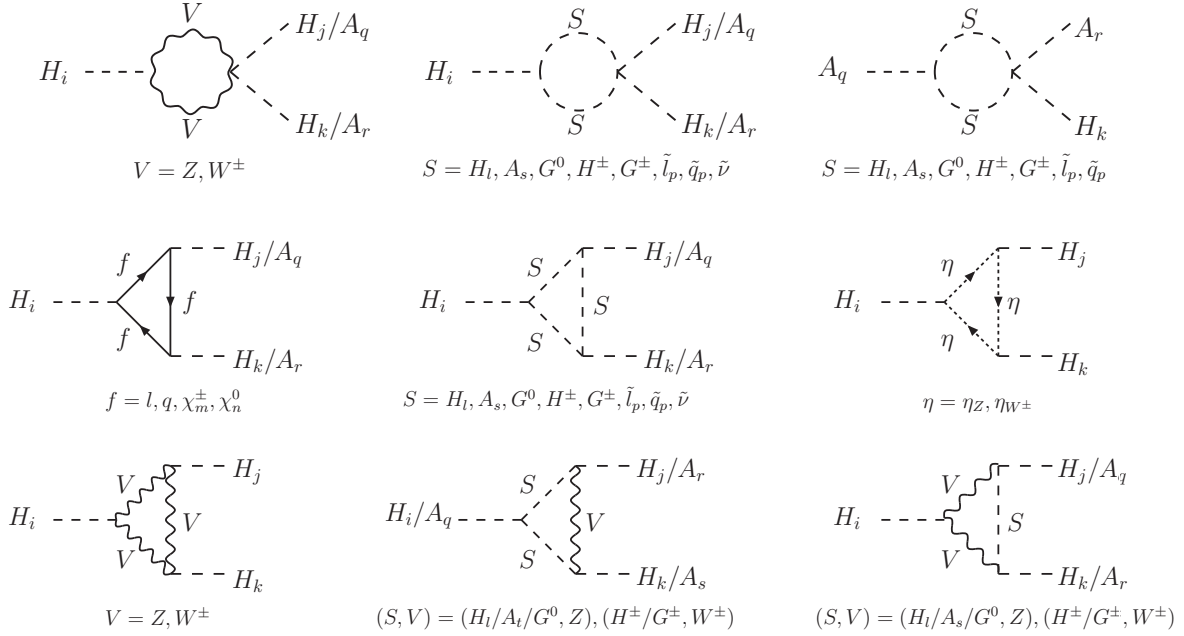


Figure 1: Generic Feynman diagrams contributing to the 1-point irreducible vertex functions. They are grouped by loops over scalars ( $S$ ), vector bosons ( $V$ ), fermions ( $f$ ) and ghost particles ( $\eta$ ).

breaks gauge invariance in the decay processes involving CP-odd Higgs bosons,  $H_i \rightarrow A_l A_m$  and  $A_2 \rightarrow A_1 H_i$ . The decay widths at one-loop level contain contributions from Feynman diagrams involving  $A_l Z$  and  $A_l G$  transitions as depicted in Fig. 2. For these contributions the following Ward Slavnov-Taylor identity ( $l = 1, 2$ ) exists,

$$\hat{\Sigma}_{a_l G}(p^2) + \frac{ip^2}{M_Z} \hat{\Sigma}_{a_l Z}(p^2) = (p^2 - m_{a_l}^2) \left( \mathcal{R}_{l1}^P f_0(p^2) + \frac{1}{2} \sin 2\beta \frac{\delta \tan \beta}{\tan \beta} \mathcal{R}_{l1}^P - \frac{1}{2} \delta Z_{a_l G} \right), \quad (42)$$

where ( $i = 1, 2, 3$ )

$$f_0(p^2) = \frac{\alpha}{4\pi s_{2W}^2} \sum_{i=1}^3 [\cos 2\beta \mathcal{R}_{i1}^S \mathcal{R}_{i2}^S + \cos \beta \sin \beta ((\mathcal{R}_{i2}^S)^2 - (\mathcal{R}_{i1}^S)^2)] B_0(p^2, M_Z^2, m_{h_i}^2), \quad (43)$$

with  $B_0(p^2, M_Z^2, m_{h_i}^2)$  denoting the scalar two-point function,  $\hat{\Sigma}_{a_l G}(p^2)$  and  $\hat{\Sigma}_{a_l Z}(p^2)$  the renormalised self-energies and  $m_{a_l}$  and  $m_{h_i}$  the CP-odd and CP-even tree-level Higgs boson masses. The rotation matrices  $\mathcal{R}^S$  and  $\mathcal{R}^P$  have been defined in Eq. (10) and Eq. (11), respectively. By

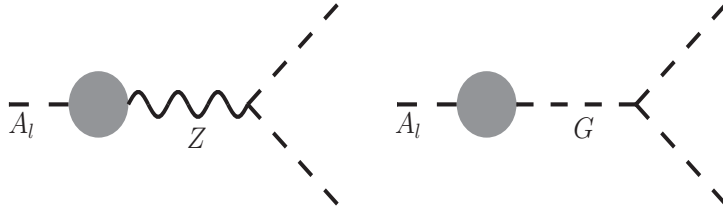


Figure 2: Generic one-loop Feynman diagrams involving  $A_l Z$  and  $A_l G$  transitions contributing to  $\delta M^{G,Z \text{ mix}}$ .

$\delta \tan \beta$  we denote the counterterm of  $\tan \beta$  and by  $\delta Z_{A_i G}$  the wave function counterterms. We have computed these identities using the same method as in Ref. [36] and checked them numerically at arbitrary momentum. We use them to test gauge invariance by applying the general  $R_\xi$  gauge for the propagators of the exchanged  $Z$  and Goldstone bosons. When  $p^2$  is set equal to the loop-corrected mass squared, the right-hand side of Eq. (42) does not vanish any more and we therefore get a contribution to the amplitude from the mixing of the pseudoscalar bosons with the  $Z$  and the Goldstone boson, which depends on the gauge fixing parameters. In order to get a gauge invariant amplitude, one can use the tree-level masses for the CP-odd Higgs bosons in the  $A_i Z$  and  $A_i G$  mixing diagrams, which has been applied in [35, 37]. Alternatively, one can use the loop-corrected masses for the external particles also in these contributions, which are then computed in the unitary gauge. We have applied both methods. The difference between the two results is of higher order. In the end the  $A_i Z$  and  $A_i G$  mixing contributions are small compared to the remaining contributions to the decay amplitude.

For the determination of the loop-corrected Higgs boson masses, mixings and trilinear Higgs boson self-couplings two independent calculations have been performed. While in both calculations the necessary model file was created using the program `Sarah` [38], one of them is based on a Fortran code that uses `FeynArts-3.6` [39] to generate the Feynman diagrams, the other one uses `FeynArts-3.5`. In both calculations the amplitudes are evaluated with `FormCalc-6.1` [40], and the numerical evaluation of the loop-integrals is performed with the program `LoopTools` [40]. The required counterterms of the Higgs boson sector are supplied by two independent Mathematica programs, which determine these in the course of the calculation of the loop-corrected masses of the neutral Higgs bosons.

## 4 Numerical Analysis

### 4.1 Input Parameters and Constraints

In our numerical analysis, we use the following SM parameters [41, 42]

$$\begin{aligned} \alpha(M_Z) &= 1/128.962, & \alpha_s(M_Z) &= 0.1184, & M_Z &= 91.1876 \text{ GeV}, \\ M_W &= 80.385 \text{ GeV}, & M_t &= 173.5 \text{ GeV}, & m_b^{\overline{\text{MS}}}(m_b^{\overline{\text{MS}}}) &= 4.18 \text{ GeV}. \end{aligned} \quad (44)$$

The running strong coupling constant  $\alpha_s$  is evaluated at two-loop order in the calculation of the loop-corrected NMSSM Higgs boson masses and of the Higgs pair production cross sections. The top quark pole mass ( $M_t$ ) and the  $\overline{\text{MS}}$  bottom quark mass will be used to compute the running quark masses at the renormalisation scale  $\mu_R = M_{\text{SUSY}}$ , as described at the end of Section 2. The running bottom and top quark masses are then used in the evaluation of the loop-corrected Higgs boson masses, mixings and decay widths. The light quark masses have only a small influence on the results. They are chosen as

$$m_u = 2.5 \text{ MeV}, \quad m_d = 5 \text{ MeV}, \quad m_s = 95 \text{ MeV} \quad \text{and} \quad m_c = 1.27 \text{ GeV}. \quad (45)$$

Concerning the NMSSM sector, we set the soft SUSY breaking masses and trilinear couplings of

the third generation and the gaugino mass parameters as follows

$$\begin{aligned} M_{\tilde{L}_3} = M_{\tilde{\tau}_R} = 250 \text{ GeV}, \quad A_t = A_b = A_\tau = 1.5 \text{ TeV}, \quad M_{\tilde{Q}_3} = M_{\tilde{t}_R} = M_{\text{SUSY}}, \\ M_{\tilde{b}_R} = 1 \text{ TeV}, \quad M_1 = 162 \text{ GeV}, \quad M_2 = 340 \text{ GeV}, \quad M_3 = 1 \text{ TeV}. \end{aligned} \quad (46)$$

The soft SUSY breaking masses and trilinear couplings of the first and second generations also only slightly affect our results and have been set to

$$M_{\tilde{L}_{1,2}} = M_{\tilde{e}_R} = M_{\tilde{\mu}_R} = 2 \text{ TeV}, \quad A_{u,c} = A_{d,s} = 2 \text{ TeV}, \quad M_{\tilde{Q}_{1,2}} = M_{\tilde{u}_R} = M_{\tilde{c}_R} = 2 \text{ TeV}. \quad (47)$$

These values guarantee a supersymmetric particle spectrum which is in accordance with present LHC searches for SUSY particles [43].

Over the remaining NMSSM parameters we perform a scan with the following restrictions: The SUSY mass scale  $M_{\text{SUSY}}$  which controls the soft SUSY breaking masses of the third generation is chosen such that we can have light stop and sbottom masses which are still in accordance with the LHC exclusion limits [44]. We vary it as

$$650 \text{ GeV} \leq M_{\text{SUSY}} \leq 750 \text{ GeV}. \quad (48)$$

This leads to stop and sbottom masses of

$$469 \text{ GeV} \leq M_{\tilde{t}_1} \leq 607 \text{ GeV}, \quad 823 \text{ GeV} \leq M_{\tilde{t}_2} \leq 902 \text{ GeV}, \quad (49)$$

$$655 \text{ GeV} \leq M_{\tilde{b}_1} \leq 752 \text{ GeV}, \quad 1000.2 \text{ GeV} \leq M_{\tilde{b}_2} \leq 1000.3 \text{ GeV}. \quad (50)$$

The value of  $\tan \beta$  is chosen as

$$2 \leq \tan \beta \leq 10. \quad (51)$$

Low values of  $\tan \beta$  allow to maximize the tree-level mass of the lightest Higgs boson so that the Higgs mass corrections which are governed by the stop sector can be kept small enough to avoid large fine-tuning [45, 46]. Also the effective parameter  $\mu_{\text{eff}}$  is taken as small as possible for fine-tuning reasons, and is varied in the range

$$100 \text{ GeV} \leq \mu_{\text{eff}} \leq 200 \text{ GeV}. \quad (52)$$

To keep  $\lambda$  and  $\kappa$  in the perturbative regime up to the GUT scale we choose

$$0 \leq \lambda, \kappa \leq 0.7 \quad \text{with} \quad \sqrt{\lambda^2 + \kappa^2} < 0.7. \quad (53)$$

The charged Higgs boson mass (which replaced the original parameter  $A_\lambda$ ) is varied in a range respecting the experimental exclusion limits [47],

$$160 \text{ GeV} \leq M_{H^\pm} \leq 1 \text{ TeV}. \quad (54)$$

Finally, the tree-level mass of the lightest pseudoscalar Higgs boson,  $m_{a_1}$ , is chosen in the interval

$$0 \text{ GeV} \leq m_{a_1} \leq 1 \text{ TeV}. \quad (55)$$

The variation of  $m_{a_1}$  instead of  $A_\kappa$  allows a better control over the mass of the singlet-like CP-odd Higgs boson, which can be  $A_1$  or  $A_2$  depending on the parameter set. Among the points that have been generated in the above parameter space, we selected only those which satisfy the following constraints arising from the LHC discovery of a SM-like Higgs boson [1, 2] and from the exclusion limits reported by LEP, Tevatron and LHC:

- 1.) One of the scalar Higgs bosons  $H_1$  or  $H_2$ , denoted by  $h$  in the following, is demanded to have a loop-corrected mass in the range

$$124 \text{ GeV} \leq M_h \leq 127 \text{ GeV} . \quad (56)$$

- 2.) We check our parameter points for compatibility with the experimental best fit values to the signal strengths [48, 49]. For this we define the quantity,

$$R_{XX}(h) = \frac{\sigma(gg \rightarrow h)}{\sigma(gg \rightarrow H_{\text{SM}})} \times \frac{\text{BR}(h \rightarrow XX)}{\text{BR}(H_{\text{SM}} \rightarrow XX)} \equiv R_\sigma(h) \times R_{XX}^{\text{BR}}(h) , \quad (57)$$

which measures the rate of an NMSSM Higgs boson  $h$  with mass near 125 GeV, produced in gluon fusion and decaying into the final state  $XX$ , compared to the corresponding value of the SM Higgs boson  $H_{\text{SM}}$  with same mass as  $h$ . Here,  $\text{BR}(H \rightarrow XX)$  denotes the branching ratio of the decay of the Higgs boson  $H$  ( $H = H_{\text{SM}}, h$ ) into the final state  $XX$  and  $\sigma$  is the production cross section via gluon fusion. Since for a SM-like Higgs boson the main production mechanism is given by gluon fusion, it is sufficient to restrict ourselves to gluon fusion in the production. The SUSY and NMSSM Higgs boson particle spectrum has been calculated with our own Fortran code, which also calculates the loop-corrected Higgs boson masses that are needed *e.g.* for the external particles in the calculation of the Higgs-to-Higgs decays, *cf.* section 3. The branching ratios and partial widths are evaluated with a Fortran code which we have written ourselves by modifying the program `HDECAY` [50, 51] to the case of NMSSM Higgs bosons. We thus include the most important higher order QCD corrections in the decay widths.<sup>1</sup> We use the ratio of the partial decay width of  $h$  into gluons with respect to the one of the SM Higgs boson in order to approximate  $R_\sigma(h)$  in Eq. (57).

In the NMSSM, there can be scenarios where two Higgs bosons are close in mass so that the signal is not built up by a single Higgs boson but by a superposition of the rates of neighbouring Higgs bosons, which depends of course on the experimental resolution in the respective final state. In order to compare with the experimentally measured signal strengths  $\mu_{XX}$  in the various final states, we introduce the reduced cross sections  $\mu_{XX}$  which are built up by the superposition of the rates from an NMSSM  $h$  boson near 125 GeV and other NMSSM Higgs bosons  $\Phi = H_i, A_l$  ( $i = 1, 2, 3, l = 1, 2$ ) close in mass. It is given by

$$\mu_{XX}(h) \equiv R_\sigma(h) R_{XX}^{\text{BR}}(h) + \sum_{\substack{\Phi \neq h \\ |M_\Phi - M_h| \leq \delta}} R_\sigma(\Phi) R_{XX}^{\text{BR}}(\Phi) F(M_h, M_\Phi, d_{XX}) . \quad (58)$$

By  $\delta$  we denote the mass resolution in the respective final state  $XX$ . The superposition with the non- $h$  Higgs bosons is weighted with a Gaussian weighting function  $F(M_h, M_\Phi, d_{XX})$ . The parameter  $d_{XX}$ , which influences the width of the weighting function, takes into account the experimental resolution of the different channels.<sup>2</sup>

In order to comply with the recent Higgs search results of the best fits to the signal strengths in the  $\gamma\gamma$  and massive gauge boson  $WW, ZZ$  final states, we only keep parameter points

---

<sup>1</sup>We have not included electroweak corrections, as they cannot easily be transferred from the SM/MSSM to the NMSSM. QCD corrections on the other hand do not involve Higgs couplings, so that they can readily be taken over for the NMSSM.

<sup>2</sup>We follow here the approach implemented in the program package `NMSSMTools` [52, 53], which is based on NMSSM extensions of the Fortran codes `HDECAY` [50, 51] and `SDECAY` [51, 54].

which lead to a Higgs mass spectrum with the following conditions:

Conditions on the parameter scan:

$$\begin{aligned}
&\text{At least one CP-even Higgs boson } h \text{ with:} && 124 \text{ GeV} \lesssim M_h \lesssim 127 \text{ GeV} \\
&\text{For } 124 \text{ GeV} \lesssim M_h = M_{H_{\text{SM}}} \lesssim 127 \text{ GeV} && \\
&\text{the reduced cross sections for } \gamma\gamma \text{ must fulfill:} && \mu_{\gamma\gamma}(h) \geq 0.8 \\
&\text{the reduced cross sections for } ZZ, WW \text{ must fulfill:} && 0.8 \leq \mu_{ZZ}(h), \mu_{WW}(h) \leq 1.2
\end{aligned} \tag{59}$$

For the rates in the  $b\bar{b}$  and  $\tau\bar{\tau}$  final states, we do not apply any restriction since these channels suffer from large uncertainties up to date.

- 3.) We use `HiggsBounds-3.8.1` [55] to verify that the Higgs mass spectrum resulting from the respective chosen parameter set is allowed by the published exclusion bounds from the Higgs searches at LEP, Tevatron and LHC.<sup>3</sup> Otherwise the parameter set is rejected.

If not stated otherwise, in the following numerical analysis we keep only those parameter sets of our parameter scan which fulfill the restrictions 1.)-3.). Furthermore, we call the NMSSM Higgs boson, which fulfills the conditions Eq. (56) and Eq. (59), *i.e.* which has a mass value around 125 GeV and rates compatible with the LHC searches in the gauge boson final states, SM-like and denote it by  $h$ . Note, however, that calling a Higgs boson SM-like according to these definitions does not necessarily imply that it has SM-like couplings. It is only the reduced signal strengths which we demand to be SM-like.

## 4.2 Effective trilinear Higgs couplings

Before we investigate the effect of the one-loop corrected trilinear Higgs boson self-couplings on Higgs boson phenomenology, namely on Higgs-to-Higgs decays and Higgs boson pair production, we discuss in this subsection the effective trilinear Higgs couplings, that are defined in the following.

In the SM, the trilinear Higgs coupling at tree-level is given by

$$\lambda_{SM}^{\text{tree}} = \frac{3M_H^2}{v}, \tag{60}$$

where  $M_H$  is the physical SM Higgs boson mass and  $v = 246$  GeV is the vacuum expectation value. In the NMSSM we have

$$v = \sqrt{v_u^2 + v_d^2}. \tag{61}$$

We define the one-loop corrected effective trilinear SM Higgs coupling as the one which includes the one-loop contributions evaluated at zero external momenta. The calculation is performed by applying the on-shell renormalisation scheme for  $e, M_Z, M_W, M_H$  and the tadpole as well as for the Higgs field. For Higgs boson masses below 160 GeV, the effective trilinear Higgs coupling can be approximated by

$$\lambda_{SM}^{\text{eff}} = \lambda_{SM}^{\text{tree}} \left( 1 - \frac{\alpha M_t^4}{\pi M_H^2 M_W^2 s_W^2} \right), \tag{62}$$

---

<sup>3</sup>We have included the latest results of the exclusion bounds in the dominant channels, *i.e.*  $\gamma\gamma$  [56],  $ZZ$  [57] and  $W^+W^-$  [58].

with  $s_W \equiv \sin \theta_W$  and  $\theta_W$  denoting the weak angle. This coincides with the result of Ref. [59]. For a heavier Higgs boson, diagrams with Higgs bosons inside the loops give important contributions of order  $\mathcal{O}(M_H^4, M_H^2 M_t^2)$ . As we only consider SM Higgs boson masses of 125 GeV, we can use the approximation Eq. (62).

The one-loop corrected effective trilinear Higgs self-couplings of the NMSSM are defined in the same way as the SM one. This means that the expressions Eq. (39)-Eq. (41), which are nothing else but the one-loop corrected Higgs boson self-couplings, have to be evaluated at zero external momenta, and the wave function renormalisation matrix,  $\mathbf{Z}^{S/P}$ , has to be replaced by the rotation matrix  $\mathbf{Z}^{S/P}(p^2 = 0)$  of the loop-corrected renormalised CP-even/odd Higgs boson mass matrices evaluated at zero external momentum,  $\hat{M}_{S/P}^2(0)$ . The latter have been defined in Eq. (17)/Eq. (18). On the other hand, the tree-level effective trilinear Higgs couplings of the NMSSM are the tree-level couplings dressed by the loop-corrected rotation matrices at zero external momentum  $\mathbf{Z}^{S/P}(0)$ . In the same way we have applied the loop-corrected rotation matrices  $\mathbf{Z}^{S/P}(0)$  in the couplings of the Higgs bosons to the remaining SM particles and implemented these in our modified version of the program HDECAY, which we use to calculate the branching ratios of the NMSSM Higgs bosons. With these definitions the effective couplings are real. If not stated otherwise we will use them in the following in particular in the computation of the Higgs pair production processes.

We first discuss the SM limit. In the framework of the MSSM, it has been shown in [60, 61] that both the tree-level and the loop-corrected Higgs self-couplings (the trilinear and the quartic one) of the lightest MSSM Higgs boson converge to the corresponding SM ones in the decoupling limit, *i.e.*  $M_{H_{\pm}} \gg M_Z$ . This feature is not shared by the NMSSM, also not at tree level, due to the mixing with the singlet component. Figure 3 shows the difference between the effective trilinear Higgs self-coupling of the lightest NMSSM Higgs boson  $H_1$  and the one of the SM Higgs boson. The difference is evaluated for the tree-level couplings normalised to the tree-level SM effective coupling as well as for the one-loop couplings normalised to the one-loop SM effective coupling. Hence ( $H_1 \equiv h$ )

$$\frac{\Delta \lambda^{\text{eff}}}{\lambda_{\text{SM}}^{\text{eff}}} = \begin{cases} \frac{\lambda_{hhh}^{\text{eff,tree}} - \lambda_{\text{SM}}^{\text{eff,tree}}}{\lambda_{\text{SM}}^{\text{eff,tree}}} & \text{at tree-level} \\ \frac{\lambda_{hhh}^{\text{eff,1l}} - \lambda_{\text{SM}}^{\text{eff,1l}}}{\lambda_{\text{SM}}^{\text{eff,1l}}} & \text{at one-loop level.} \end{cases} \quad (63)$$

The normalised deviation is shown as a function of the singlet admixture, which is given by the rotation matrix element  $\mathcal{R}_{13}^S$ . We have chosen a scenario where the lightest NMSSM Higgs boson  $H_1$  is SM-like according to our definition at the end of Subsection 4.1. This means that it has a mass of about 125 GeV and that the signal strengths in the gauge boson final states are SM-like. Note, however, that this does not imply that  $H_1$  has SM-like couplings, in particular not for large singlet admixtures. The criteria on the reduced signal strengths are in this case fulfilled only due to the superposition with a second CP-even Higgs boson which is close in mass and which has SM-like couplings. In order to get different values for the mixing we have varied the trilinear soft SUSY breaking coupling  $A_t$  of the stop sector, while taking care to keep  $H_1$  at 125 GeV and to fulfill the constraints on the reduced signal strengths. As can be inferred from the figure,  $|\Delta \lambda^{\text{eff}}/\lambda_{\text{SM}}^{\text{eff}}|$  increases with the mixing, both at tree-level and at one-loop level. It can become as large as 1.4 at



loop level, and as large as 1.75 at tree-level, provided that  $H_1$  is rather singlet-like.<sup>4</sup> In the limit of zero singlet admixture,  $H_1 \equiv h$  becomes effectively MSSM-like, and with the chosen large charged Higgs boson mass of  $M_{H^\pm} = 990$  GeV we are in the SM-limit. In this SM-limit, the NMSSM trilinear Higgs self-coupling coincides with the SM effective self-coupling, as expected.

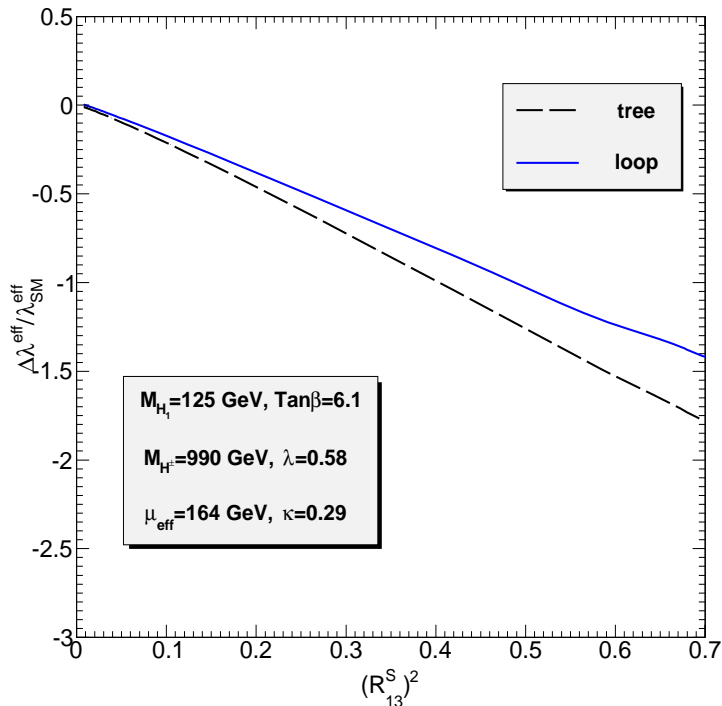


Figure 3: Normalised deviation of the trilinear Higgs self-coupling of the SM-like NMSSM Higgs boson, here  $H_1 = h$ , from the corresponding SM coupling,  $\Delta\lambda^{\text{eff}}/\lambda_{\text{SM}}^{\text{eff}}$ , with  $\Delta\lambda^{\text{eff}} = \lambda_{hhh}^{\text{eff}} - \lambda_{\text{SM}}^{\text{eff}}$ , as a function of the singlet admixture squared of  $H_1$ ,  $(R_{13}^S)^2$ , both for tree-level and one-loop corrected self-couplings. In this figure  $A_t$  is varied such that  $H_1$  is kept SM-like according to our definitions in subsection 4.1. The remaining parameters have been chosen as given in Eqs. (44)-(47). The  $\overline{\text{DR}}$  renormalised parameters are taken at the renormalisation scale,  $\mu_R = M_{\text{SUSY}} = 700$  GeV.

The one-loop corrected NMSSM effective trilinear Higgs couplings receive significant contributions from the diagrams with (s)top quarks in the loops.<sup>5</sup> There can be, however, extremely large contributions from the triangle diagrams with light singlet-like bosons in the loop. In case  $H_2$  is the Higgs boson with mass around 125 GeV,  $A_1$  and  $H_1$  have to be singlet-like in order to avoid the exclusion limits on light Higgs boson masses. The analytic expressions for the one-loop contribution

<sup>4</sup>In fact, with rising singlet admixture the CP-even Higgs bosons  $H_1$  and  $H_2$ , which are close in mass, interchange their roles. For large singlet admixtures, the deviation from the SM value of the trilinear Higgs self-coupling at large masses  $M_{H^\pm}$  is hence only an artefact of  $H_1$  losing its role as Higgs boson with SM-like couplings.

<sup>5</sup>For small values of  $\tan\beta$ .

$\delta\lambda^{A_1}$  and  $\delta\lambda^{H_1}$  of  $A_1$ , respectively  $H_1$ , running in the loop, can be cast into the form ( $i = 1, 2, 3$ )

$$\delta\lambda_{H_i H_i H_i}^{A_1} = \frac{1}{16\pi^2} \left( \sum_{j=1}^3 \mathbf{Z}_{ij}^S \lambda_{h_j a_1 a_1} \right)^3 \frac{1}{2m_{a_1}^2}, \quad (64)$$

$$\delta\lambda_{H_i H_i H_i}^{H_1} = \frac{1}{16\pi^2} \left( \sum_{j=1}^3 \mathbf{Z}_{ij}^S \lambda_{h_j h_1 h_1} \right)^3 \frac{1}{2m_{h_1}^2}, \quad (65)$$

where we use tree-level masses  $m_{a_1}$ ,  $m_{h_1}$ , respectively, for the Higgs bosons inside the loops, and  $\lambda$  denotes the tree-level trilinear couplings. These contributions hence blow up when  $m_{a_1}$  or  $m_{h_1}$

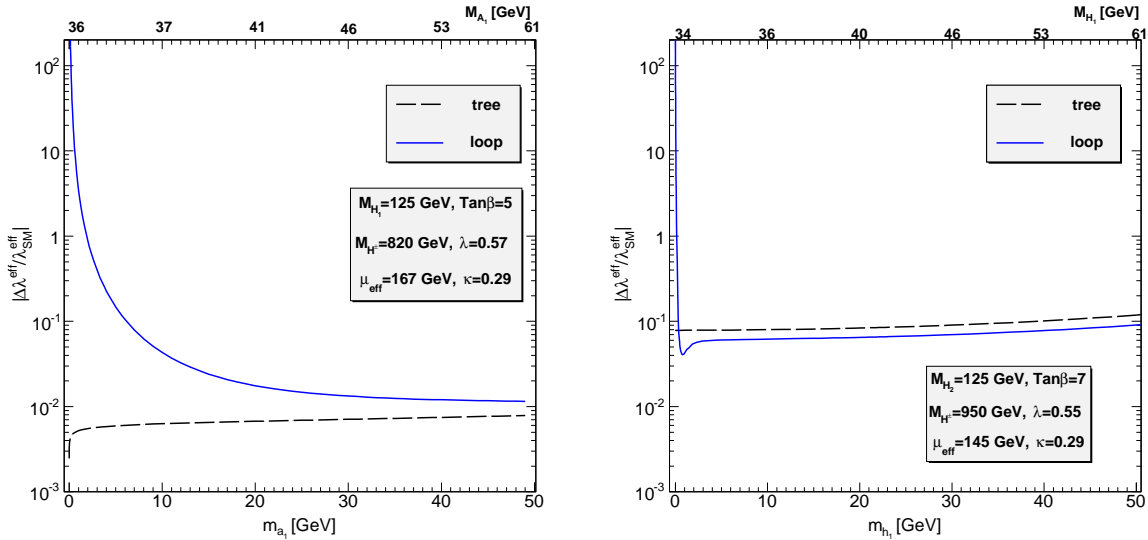


Figure 4: Absolute value of  $\Delta\lambda^{\text{eff}}/\lambda_{\text{SM}}^{\text{eff}}$  for tree-level couplings (dashed) and one-loop corrected couplings (full) as a function of the tree-level lightest CP-odd Higgs mass  $m_{a_1}$  for a 125 GeV  $H_1$  (left) and as a function of the tree-level lightest CP-even Higgs mass  $m_{h_1}$  for a 125 GeV  $H_2$  (right). The scales on top of each figure refer to the loop-corrected mass  $M_{A_1}$  (left) and  $M_{H_1}$  (right). The parameters have been chosen as specified in Eqs. (44)-(47), and the renormalisation scale has been set  $\mu_R = M_{\text{SUSY}} = 700$  GeV.

become small while the trilinear couplings remain non vanishing. We show examples of such large contributions to  $\lambda_{\text{NMSSM}}^{\text{eff}}$  for  $H_1$  having a mass around 125 GeV in Fig. 4 (left) and for a 125 GeV  $H_2$  in Fig. 4 (right). In these figures we use again the quantity  $\Delta\lambda^{\text{eff}}/\lambda_{\text{SM}}^{\text{eff}}$  to characterise the differences between the effective tree-level and one-loop corrected NMSSM couplings and the corresponding SM ones. In Fig. 4 (left) large contributions only arise from a light singlet-like  $A_1$ , as it is the only Higgs boson with mass smaller than  $H_1$ . Figure 4 (right) shows the case of  $H_2$  having a mass near 125 GeV, so that large contributions can arise both from a very light  $A_1$  and  $H_1$ . As can be inferred from the figures, while the tree-level couplings are small, the loop corrections become extremely large for light singlet masses. (The drop of the tree-level coupling in Fig. 4 (left) is due to a cancellation between the various terms entering the coupling. The kink in Fig. 4 (right) is due to a sign change in  $\Delta\lambda^{\text{eff}}$ .) We note, however, that the existence of these huge contributions is not compatible with the constraints in subsection 4.1, Eq. (59), on the 125 GeV Higgs boson. The reason is the following. When the tree-level mass  $m_{a_1}$  ( $m_{h_1}$ ) is very small, its loop-corrected

mass is still small enough for the decay  $H_1 \rightarrow A_1 A_1$  ( $H_2 \rightarrow H_1 H_1$ ) being kinematically possible. (The upper scales of Figs. 4 show, respectively, the loop-corrected masses  $M_{A_1}$  and  $M_{H_1}$ .) These decays turn out to be important so that the branching ratios of the decays into  $\gamma\gamma$ ,  $WW$  and  $ZZ$  become very much suppressed and the decay rates in these final states are not compatible any more with the best fit values to these final state signal strengths given by the experiment. A discussion on non-decoupling effects of the one-loop trilinear couplings can also be found in [62], without, however, taking into account the possibility of large singlet contributions.

### 4.3 Results for Higgs boson decays

In this subsection we show the effect of the one-loop corrected trilinear Higgs self-couplings on the branching ratios of heavy Higgs bosons into a pair of lighter Higgs bosons. These decays play a role in the search for the heavy Higgs bosons, which can possibly be detected at the LHC via

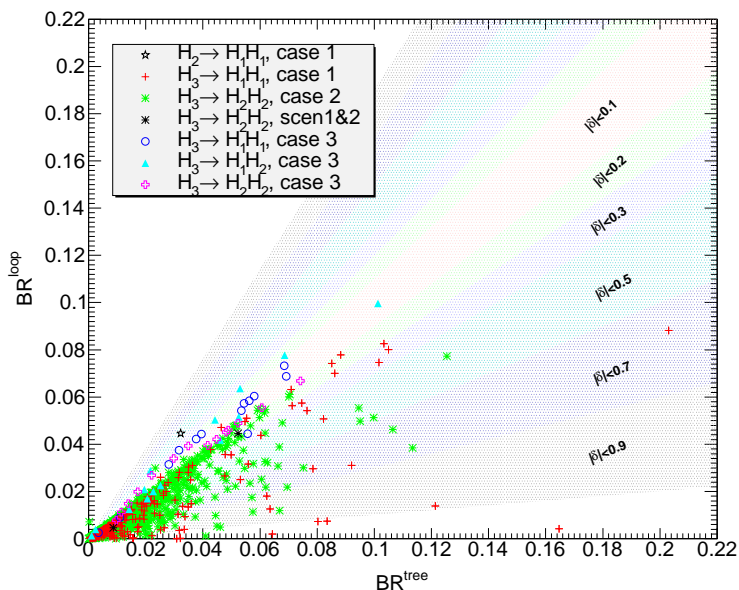


Figure 5: The branching ratio of heavier CP-even Higgs bosons,  $H_2$  or  $H_3$ , decaying into two SM-like Higgs bosons at loop level versus the tree-level branching ratio, for scenarios with  $h \equiv H_1$  (case 1),  $h \equiv H_2$  (case 2, scen1, scen2) as well as  $H_1$  and  $H_2$  close in mass near 125 GeV (case 3). The difference between the one-loop and the tree-level branching ratio is quantified by  $\delta \equiv (BR^{\text{loop}} - BR^{\text{tree}})/BR^{\text{tree}}$ . The colored areas refer to different ranges of  $\delta$ .

their decay into a pair of lighter Higgs bosons, which then subsequently decay further into SM particles. Figure 5 shows the branching ratios of the decay of a heavy CP-even Higgs boson,  $H_2$  or  $H_3$  depending on the scenario, into two SM-like Higgs bosons including loop-corrected trilinear Higgs self-couplings, as defined in Eq. (39), versus the branching ratio evaluated with tree-level trilinear couplings (*cf.* Eq. (39) without the 1-point irreducible contributions). The three different cases refer to scenarios with the SM-like Higgs boson being  $H_1$ ,  $h \equiv H_1$  (case 1), with  $H_2$  being SM-like,  $h \equiv H_2$  (case 2), and with two light Higgs bosons  $H_1$  and  $H_2$  both having mass around 125 GeV and the combined Higgs rates being compatible with the SM rates (case 3). As can be inferred from the figure, which only includes scenarios compatible with our constraints, the loop-

corrected trilinear Higgs coupling has the tendency to decrease the branching ratio compared to the tree-level result. The deviations can be as large as 90% in terms of the tree-level branching ratio, in some cases even higher. Also shown by black filled stars are two scenarios, where the SM-like Higgs boson is given by  $H_2$ . The corresponding tree-level and loop corrected branching ratios amount to

$$\begin{aligned} (\text{BR}^{\text{loop}}, \text{BR}^{\text{tree}})_{H_3 \rightarrow H_2 H_2} &= (4.7 \times 10^{-3}, 8.7 \times 10^{-3}) & \text{scen1} \\ (\text{BR}^{\text{loop}}, \text{BR}^{\text{tree}})_{H_3 \rightarrow H_2 H_2} &= (4.5 \times 10^{-2}, 5.2 \times 10^{-2}) & \text{scen2} \end{aligned} \quad (66)$$

These two scenarios scen1 and scen2 have the characteristic feature of being excluded if loop corrections are not taken into account. In scen1 the tree-level branching ratio of the SM-like  $H_2$  decay into  $H_1 H_1$  is as large as 0.02. This decreases the branching ratios into the other SM particles so that the scenario would be excluded because the reduced signal strength in the  $WW$  final state drops below 0.8 and the constraints Eq. (59) are not fulfilled any more. Only the inclusion of the loop corrections decreases the branching ratio into  $H_1 H_1$  to  $2 \cdot 10^{-4}$  so that the scenario meets the constraints Eq. (59). In scen2 it is the branching ratio of the decay  $H_2 \rightarrow A_1 A_1$  which is as large as 0.26 at tree-level compared to 0.1 after the inclusion of loop corrections, so that the scenario is not valid at tree-level due to too small reduced signal strengths in the  $WW$  and  $ZZ$  final states, unless loop corrections are included. These examples demonstrate the importance of including the higher order corrections in order to properly interpret the NMSSM spectrum with respect to the experimental findings.

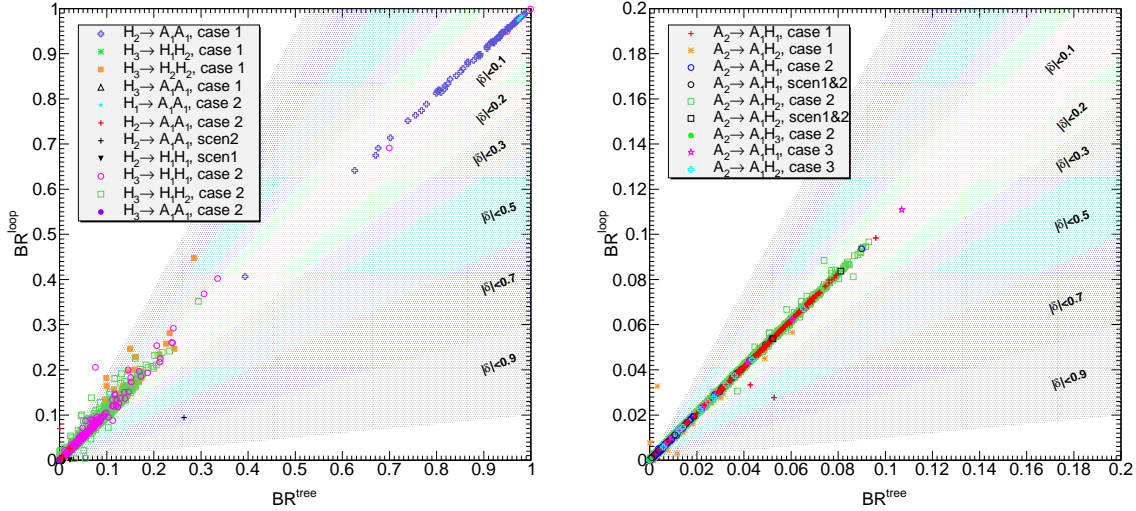


Figure 6: Same as Fig. 5 but for all other possible two-body decay modes of heavy scalar (left) and pseudoscalar (right) Higgs bosons into two lighter ones.

In Fig. 6 left (right) we show the remaining possible branching ratios of heavy scalar (pseudoscalar) Higgs bosons into a pair of lighter Higgs bosons. In the left figure, the full black triangle corresponds to the decay  $H_2 \rightarrow H_1 H_1$  of scen1 and the black cross to the decay of  $H_2 \rightarrow A_1 A_1$  of scen2. The significant loop corrections leading to deviations of up to 90%, respectively 70%, in terms of the corresponding tree-level decay are crucial for the two scenarios to be still in accordance with the LHC constraints Eq. (59). In the right figure, the black squares are the branching ratio

values of the decay  $A_2 \rightarrow A_1 H_2$  in scen1 and scen2, respectively. In this decay the deviations between the tree-level and loop-corrected branching ratios are small, less than 0.1 for both scenarios.

Figure 7 shows the branching ratio of the SM-like  $H_2$  decay into  $H_1 H_1$  as a function of  $\tan \beta$  (left) and of  $\lambda$  (right), evaluated at tree-level and at loop level. All the box points are allowed points, while the red star points do not fulfill our constraints. The figure shows that there are scenarios that would be excluded at tree-level, but are allowed once loop corrections are taken into account, which suppress the non-SM decays into Higgs boson pairs, so that the branching ratios into the SM particles remain compatible with the experimental constraints. The point of scen1 in Fig. 5 corresponds to  $\tan \beta = 3.37$  in Fig. 7 (left) and to  $\lambda = 0.46$  in Fig. 7 (right). The plots illustrate once more the importance of loop corrections when considering a specific model in light of the experimental results. As can be inferred from the figure, the loop corrections not only change the absolute value of the branching ratio but also shift the minimum to different  $\lambda$  values. The corresponding plots for a variation of the other parameters  $\kappa$ ,  $A_\kappa$ ,  $\mu_{\text{eff}}$  or  $M_{H^\pm}$  show a similar behaviour.

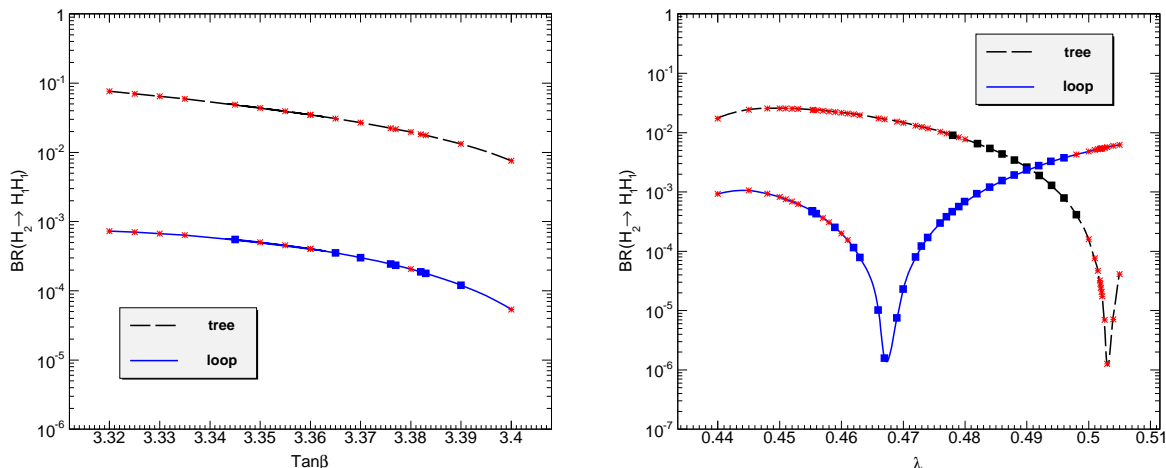


Figure 7: Branching ratio of  $H_2$  with mass around 125 GeV into two light Higgs bosons  $H_1$ , at tree-level (dashed/black) and including loop corrections (full/blue) as a function of  $\tan \beta$  (left) and of  $\lambda$  (right). Lines are there to guide the eye. Box (star) points: allowed (excluded) due to the constraints Eq. (59).

#### 4.4 Pair production of neutral Higgs bosons at the LHC

We apply the results of our calculation of the loop-corrected Higgs boson self-couplings to the pair production of neutral Higgs bosons at the LHC in order to study the effects of the higher order corrections. Higgs pair production processes are important as they give access to the trilinear Higgs self-couplings. The measurement of the trilinear and quartic Higgs self-interactions allows for the reconstruction of the Higgs potential which represents the ultimate check in the program of the experimental verification of the Higgs mechanism [5, 6]. The main contribution to Higgs pair production at the LHC comes from  $gg$  fusion [63–65]. Higgs pair production processes through vector boson fusion [66], double Higgs-strahlung [67] and associated production of a Higgs boson pair with  $t\bar{t}$  [68] are less important [8] so that we focus here on the gluon fusion channel, namely

the production of a pair of SM-like Higgs bosons in the framework of the NMSSM.

#### 4.5 SM-like Higgs boson pair production through $gg$ fusion

At leading order, the gluon fusion process into two SM-like Higgs bosons  $H_i \equiv h$  ( $i = 1, 2$  depending on the chosen parameter set),

$$gg \rightarrow H_i H_i, \quad H_i \equiv h, \quad (67)$$

consists of triangle, box and two-point contributions mediated by top and bottom (s)quarks, *cf.* Fig. 8. The diagrams are similar to the MSSM case [64, 65], except for the ones involving

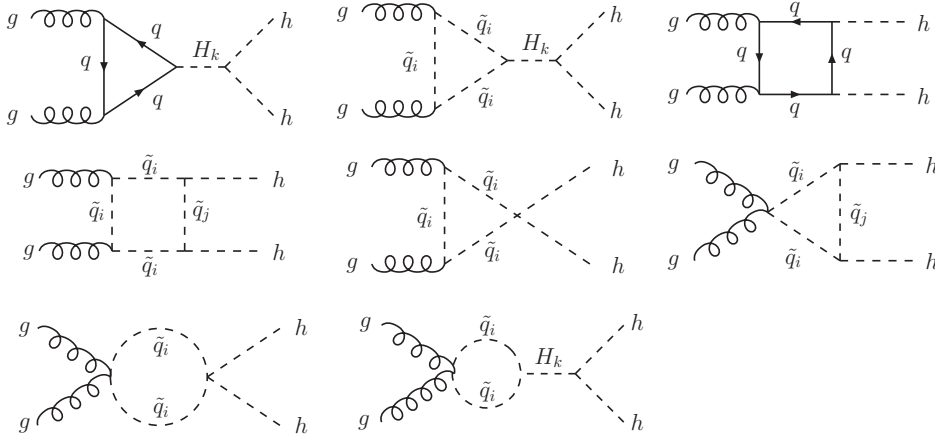


Figure 8: Generic diagrams contributing to pair production of a SM-like NMSSM Higgs boson  $h$  in gluon fusion. The loops involve top and bottom (s)quarks,  $q = t, b$ ,  $\tilde{q} = \tilde{t}, \tilde{b}$ ,  $i, j = 1, 2$ . The  $s$ -channel diagrams proceed via  $H_k = H_1, H_2, H_3$ , with one of these being the SM-like  $h$ , depending on the parameter choice.

a scalar Higgs boson in the  $s$ -channel, which gets contributions from all possible three neutral NMSSM Higgs bosons, that subsequently split via the corresponding trilinear Higgs coupling into the final state Higgs pair. Thus the  $hh$  production involves the trilinear Higgs self-couplings  $\lambda_{hhh}$  and  $\lambda_{hhH_k \neq h}$  ( $k = 1, 2, 3 \neq i$ ). The NLO QCD corrections have been calculated both for the SM and the MSSM case in the limit of heavy loop particle masses. The corrections are large, of  $\mathcal{O}(100\%)$  [65], and therefore have to be taken into account for a realistic assessment of the process. We use the public Fortran code `HPAIR` [69] which computes the QCD corrected gluon fusion processes into pairs of Higgs bosons within the SM and the MSSM, by applying the low-energy theorem. As claimed in [65], this approximation is good for small values of  $\tan \beta$  in the MSSM and for Higgs boson masses below  $2M_t$ .<sup>6</sup> This is the case for the here considered pair production of a SM-like NMSSM Higgs boson, hence with mass of about 125 GeV. Furthermore, in the NMSSM small  $\tan \beta$  values are preferred in this case. We have modified the code `HPAIR` to include the additional contributions to the triangle diagrams from the enlarged Higgs sector of the NMSSM and by replacing the involved Higgs Yukawa and trilinear Higgs couplings with the appropriate NMSSM Higgs couplings as discussed in subsection 4.2.

In the following, we present results for the pair production of two  $H_1 \equiv h$  SM-like Higgs bosons,  $gg \rightarrow hh$ . The scan performed in the NMSSM parameter space resulted in numerous scenarios,

<sup>6</sup>For further discussion of the application of the low-energy theorem to single and double Higgs production, see [70].

where the heavier scalar Higgs bosons can decay into two on-shell Higgs bosons  $hh$ , leading to resonantly enhanced contributions to the total pair production cross section. The program `HPAIR` computes the resonantly enhanced diagrams together with the remaining diagrams up to NLO QCD by making use of Breit-Wigner propagators for the intermediate Higgs bosons. Alternatively, the non-resonant contributions can be calculated by `HPAIR` at NLO QCD while the resonant ones are obtained by multiplying the cross section of a singly produced heavy Higgs boson with its branching ratio into  $hh$ . For comparison, we have also calculated the cross section in this approach, which of course neglects off-shell effects and interference terms between non-resonant and resonant contributions. The cross section for single Higgs production is obtained with the Fortran code `HIGLU` [71] and is calculated at NLO QCD to match the same order in  $\alpha_s$  as in Higgs pair production.<sup>7</sup> In `HIGLU` the Higgs Yukawa couplings have been replaced by the corresponding couplings of the produced NMSSM Higgs boson. The non-resonant and resonant contributions are then summed up to get the total cross section. We have compared the results obtained within the two approaches, and the difference has been found to be less than 10% for our scenarios. Note, that the theoretical uncertainty on the NLO QCD double Higgs production cross section due to unknown higher order corrections [65] is larger than for single Higgs production at NLO QCD [75]. All results presented hereafter have been obtained with `HPAIR`. We emphasize that, if not stated otherwise, in our calculation we have included the loop-corrected effective trilinear Higgs couplings, presented in subsection 4.2, and the involved Higgs bosons both in the final state and in the  $s$ -channel exchange are the loop-corrected Higgs states. All involved loop quantities are taken at zero external momentum.

The hadronic cross sections for SM-like Higgs boson pair production have been computed with MSTW 2008 NLO parton distribution functions (PDF) [76]. The factorization scale has been taken equal to the renormalisation scale and set equal to the invariant mass of the produced Higgs boson pair. In the code `HPAIR` top and bottom quark pole masses are used as default inputs.

## 4.6 Results for Higgs boson pair production

In Table 1 we show five sample scenarios compatible with the constraints according to Eq. (59), where  $H_1$  is SM-like (points 1,2),  $H_2$  is SM-like (points 4,5), and where  $H_1$  and  $H_2$  are close in mass with  $H_2$  being near 125 GeV (point 3). In all scenarios the  $H_3$  mass is large enough to allow for resonantly enhanced  $h$  pair production from the decay of  $H_3 \rightarrow hh$ , which can lead to a significant increase of the Higgs pair production cross section depending on the trilinear Higgs self-coupling  $\lambda_{H_3 hh}$ . Table 2 contains the cross sections including NLO QCD corrections for the production of a pair of SM-like Higgs bosons  $h$  in the five scenarios. Here  $\sigma_T$  denotes the cross sections calculated using the effective tree-level trilinear Higgs couplings  $\lambda_{\text{NMSSM}}^{\text{eff}}(\text{tree})$ , while the cross section values  $\sigma_L$  use the effective loop-corrected trilinear Higgs self-couplings  $\lambda_{\text{NMSSM}}^{\text{eff}}(\text{loop})$ . The Higgs boson masses are taken at loop level in both cases. The quantity  $\delta$  is the difference between the two cross sections in terms of  $\sigma_T$ ,

$$\delta = \frac{\sigma_L - \sigma_T}{\sigma_T}, \quad \text{with} \quad \sigma_L \equiv \sigma_{\lambda_{\text{NMSSM}}^{\text{eff}}(\text{loop})} \quad \text{and} \quad \sigma_T \equiv \sigma_{\lambda_{\text{NMSSM}}^{\text{eff}}(\text{tree})}. \quad (68)$$

---

<sup>7</sup>The program `HIGLU` includes the QCD corrections to quark loops up to NNLO QCD, taking into account the full mass dependence at NLO QCD [72]. The NLO QCD corrections to the squark loops have been implemented in the limit of heavy squark masses [73], which is a good approximation for squark masses above about 400 GeV. For the finite squark mass effects on the NLO QCD corrections to Higgs production through gluon fusion, see [74].

	$\tan \beta$	$M_{H^\pm}$	$\mu_{\text{eff}}$	$\lambda$	$\kappa$	$A_\kappa$	$M_{\text{SUSY}}$	$M_{H_1}$	$M_{H_2}$	$M_{H_3}$	$M_{A_1}$	$M_{A_2}$
Point 1	1.90	328	175	0.565	0.406	-324	710	124	146	342	324	371
Point 2	2.23	327	147	0.62	0.32	-36.0	738	125.7	143	344	153	333
Point 3	2.28	278	121	0.507	0.349	-116	706	122	125.8	294	200	280
Point 4	2.69	302	124	0.41	0.53	-533	698	111	124.2	313	296	509
Point 5	3.50	310	113	0.23	0.53	-984	686	110	124.4	311	300	871

Table 1: List of parameter points for five sample scenarios. Particle masses and dimensionful parameters are given in GeV, and  $m_t^{\text{eff}} = 155$  GeV,  $m_b^{\text{eff}} = 2.47$  GeV.

The cross section values vary significantly in the various scenarios. As can be inferred from the table, the differences in the cross sections due to the inclusion of loop corrections in the trilinear Higgs self-couplings can be substantial, ranging from nearly 40% to almost 90% in terms of the tree-level cross section for the chosen scenarios.

	$\sigma_T[\text{fb}]$	$\sigma_L[\text{fb}]$	$\delta$
Point 1	485.9(4)	55.08(4)	-0.89
Point 2	462.9(3)	254.2(2)	-0.45
Point 3	374.3(3)	175.5(1)	-0.53
Point 4	99.30(7)	28.36(2)	-0.71
Point 5	17.52(1)	24.05(2)	0.37

Table 2: The total cross sections in fb for  $pp \rightarrow H_i H_i$  through gluon fusion at  $\sqrt{s} = 14$  TeV, with  $H_i$  being the SM-like Higgs boson, evaluated with tree-level ( $\sigma_T$ ) and loop-corrected ( $\sigma_L$ ) effective trilinear Higgs couplings. The deviation in the cross sections is quantified by  $\delta = (\sigma_L - \sigma_T)/\sigma_T$ .

In Fig. 9 (left) we show the gluon fusion production cross section of a pair of SM-like Higgs bosons  $h$  calculated with the effective loop-corrected trilinear Higgs couplings, as a function of the ratio  $\lambda_{\text{NMSSM}}^{\text{eff}}(\text{loop})/\lambda_{\text{SM}}^{\text{eff}}(\text{loop})$ . Note that in the ratio  $\lambda_{\text{NMSSM}}$  refers to the trilinear Higgs self-coupling of the SM-like Higgs boson  $h$ . In the case 3 of two Higgs bosons nearby 125 GeV, the name SM-like Higgs boson refers to the Higgs boson with the most SM-like Higgs Yukawa coupling to top quarks, as this coupling determines the dominant Higgs production cross section through gluon fusion and has the major impact on the Higgs production rate. The c.m. energy has been taken to be 14 TeV. Shown are cross sections for scenarios with  $H_1 \equiv h$  (case 1), with  $H_2 \equiv h$  (case2) or with two Higgs bosons with mass around 125 GeV building up the Higgs signal (case 3). The two black stars refer to scen1 and scen2 defined in section 4.3. Also plotted as a horizontal line is the SM cross section evaluated with  $\lambda_{\text{SM}}^{\text{eff}}(\text{loop})$ . The cross section amounts to 35 fb compared to 34 fb evaluated with the tree-level coupling [8]. Furthermore, we plot as horizontal lines the results for the SM cross section in case of a variation of the effective loop-corrected trilinear coupling in terms of  $\lambda_{\text{SM}}^{\text{eff}}(\text{loop})$  by a factor 2 and by a factor -1 and in case of  $\lambda_{\text{SM}}^{\text{eff}}(\text{loop}) = 0$ . They show the sensitivity of the SM cross section to the trilinear Higgs self-coupling. In other words, they give an idea of how precisely the cross section has to be measured to achieve a certain accuracy in the trilinear SM Higgs self-coupling extracted from it. Many of the NMSSM cross section values lie nearby the SM result,



independently of the ratio between the NMSSM and SM effective loop-corrected trilinear couplings, thus mimicking the SM case. However, there are also parameter points where the NMSSM and SM cross section differ significantly, so that a distinction of the two models would be possible. Loop corrections play here a crucial role: In Fig. 9 (right) we show for the cases 1-3 the SM-like Higgs

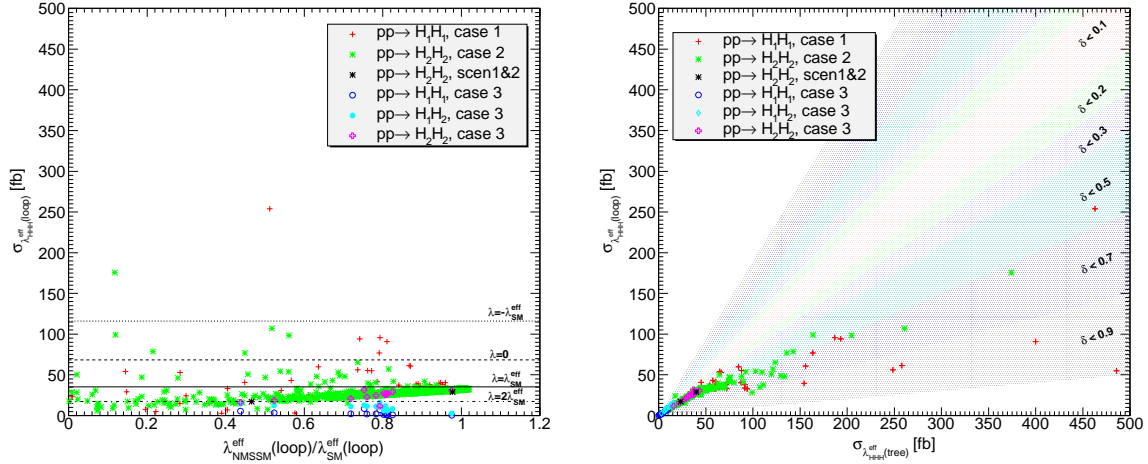


Figure 9: Cross section of SM-like double Higgs production through gluon fusion evaluated with the effective loop-corrected trilinear Higgs self-couplings as a function of  $\lambda_{\text{NMSSM}}^{\text{eff}}(\text{loop})/\lambda_{\text{SM}}^{\text{eff}}(\text{loop})$  (left) and plotted against the corresponding cross section evaluated with the tree-level effective trilinear Higgs self-couplings (right). Shown are scenarios with  $h \equiv H_1$  (case 1),  $h \equiv H_2$  (case 2, scen1, scen2),  $H_1$  and  $H_2$  close in mass near 125 GeV (case 3). Left: Also shown is the SM cross section value evaluated with the effective loop-corrected trilinear Higgs self-coupling (full line) and for Higgs self-coupling variations in terms of  $\lambda_{\text{SM}}^{\text{eff}}(\text{loop})$  by a factor 2 (dot-dashed), a factor -1 (dotted) and for vanishing coupling (dashed). Right:  $\delta \equiv (\sigma_L - \sigma_T)/\sigma_T$ .

pair production cross section of the NMSSM evaluated with the effective loop-corrected trilinear Higgs self-couplings versus the cross section evaluated with the effective tree-level couplings. The difference between the cross sections is again quantified by  $\delta$ , defined in Eq. (68). There are many scenarios with  $\delta$  up to 50% and even higher. These large deviations can be traced back to the large deviations between the tree-level and loop-corrected branching ratios of the  $H_3$  decay into two SM-like Higgs bosons  $h$ , *cf.* Fig. 5.<sup>8</sup> The fact that, depending on whether or not the loop corrections to the trilinear Higgs self-couplings are included the scenario is distinguishable or not from the SM, clearly shows the importance of the loop corrections to obtain predictions useful for the experiments.

## 5 Conclusions

The discovery of a new scalar particle by the LHC experiments ATLAS and CMS has triggered a lot of activities to determine the properties of this particle. While the analyses of the so far accumulated data strongly suggest that it is indeed the Higgs boson, *i.e.* the particle responsible for the creation of particle masses without violating gauge principles, the accumulation of more data is necessary for its interpretation with respect to other models than the SM. The question

<sup>8</sup>In the narrow-width approximation the Higgs pair production cross section is given by single Higgs production times the branching ratio  $\text{BR}(H_3 \rightarrow hh)$ .

has to be clarified if it is the Higgs boson of the SM or of some extensions beyond the SM. Among these, supersymmetric theories represent one of the most intensely studied model classes. The Higgs sector of the NMSSM consists of seven Higgs bosons entailing a rich phenomenology with possible Higgs-to-Higgs decays and resonantly enhanced double Higgs production cross sections due to heavier Higgs bosons decaying into a pair of light Higgs particles.

In order to properly interpret the experimental data and distinguish between different models the precise prediction of the Higgs parameters such as masses and couplings, including higher order corrections, is indispensable. The Higgs boson masses and Higgs self-couplings are related to each other via the Higgs potential. The prediction of loop-corrected Higgs boson masses necessitates also the inclusion of loop corrections to the Higgs self-couplings for a consistent analysis of the Higgs data. Having calculated in previous works the one-loop corrected NMSSM Higgs boson masses, in this contribution we extend our program of the calculation of loop-corrected NMSSM Higgs parameters to the computation of loop-corrected trilinear Higgs self-couplings.

The inclusion of loop corrections turns out to be important. We found for example that non-SM Higgs decays of the 125 GeV NMSSM Higgs boson into a pair of lighter Higgs bosons could be large enough to decrease the signal strengths into SM particle final states so that they are not compatible any more with the experimental results. The inclusion of loop corrections to the trilinear couplings can, however, reduce these rates to a level where the theoretical predictions are in accordance with the experimental findings. In principle this could also work the other way around, *i.e.* a scenario could be allowed if the tree-level trilinear Higgs couplings are used, but excluded in case of loop-corrected couplings. Trilinear Higgs self-couplings of course also play a role in the decays of heavier non-SM-like Higgs bosons into light Higgs pairs and their possible detection via these decays.

Trilinear Higgs self-couplings enter the production of Higgs boson pairs, so that they can be extracted from the measurement of these processes. Once the (trilinear and quartic) Higgs self-couplings are known, the Higgs potential can be reconstructed to perform the ultimate step in the experimental verification of the Higgs mechanism. We found that the inclusion of loop corrections to the trilinear Higgs self-couplings can alter the Higgs pair production cross sections through gluon fusion substantially. In many of the scenarios passing the constraints, the production cross section of a pair of SM-like Higgs bosons with mass of 125 GeV can be different enough to distinguish it from SM Higgs boson pair production. This depends of course also on the experimental accuracy which can be reached in these processes and which relies on analyses to be performed at the high-energy and high-luminosity run of the LHC.

In summary, the computation of loop corrections to Higgs boson self-couplings and their inclusion in the analyses of the experimental results is crucial, in particular for the proper interpretation of the Higgs data with respect to the exclusion or non-exclusion of NMSSM parameter scenarios and/or with respect to the correct interpretation of Higgs pair production processes.

## Acknowledgments

DTN, MMM and KW are supported by the DFG SFB/TR9 “Computational Particle Physics”. We thank Julien Baglio and Ramona Gröber for discussions. We would like to thank Pietro Slavich for the communication concerning the two-loop contribution to the NMSSM Higgs boson masses.

## A Tree-level trilinear Higgs couplings

In this appendix we present the trilinear Higgs self-couplings of the interaction eigenstates of the NMSSM Higgs sector. The tree-level trilinear couplings of the scalar mass eigenstates  $h_i$  ( $i = 1, 2, 3$ ) are obtained by applying the tree-level rotation matrices  $\mathcal{R}^S$ , Eq. (10), on the three interaction eigenstates,

$$\lambda_{h_i h_j h_k} = \mathcal{R}_{i'i'}^S \mathcal{R}_{j'j}^S \mathcal{R}_{k'k}^S \lambda_{i'j'k'}^{hhh}, \quad i, j, k = 1, 2, 3, \quad i', j', k' = 1, 2, 3. \quad (69)$$

The indices  $i', j', k'$  refer to the interaction eigenstates, and we have the following correspondences  $1 \hat{=} h_d$ ,  $2 \hat{=} h_u$ ,  $3 \hat{=} h_s$ . The couplings  $\lambda_{i'j'k'}^{hhh}$  are symmetric in the three indices. Using the short-hand notations  $c_\beta \equiv \cos \beta$ ,  $s_\beta \equiv \sin \beta$ ,  $t_\beta \equiv \tan \beta$ , we have

$$\begin{aligned} \lambda_{111}^{hhh} &= \frac{3c_\beta M_Z^2}{v}, & \lambda_{112}^{hhh} &= \left( -\frac{M_Z^2}{v} + \lambda^2 v \right) s_\beta, & \lambda_{113}^{hhh} &= \sqrt{2} \lambda \mu_{\text{eff}}, \\ \lambda_{122}^{hhh} &= \left( -\frac{M_Z^2}{v} + \lambda^2 v \right) c_\beta, & \lambda_{123}^{hhh} &= -\frac{A_\lambda \lambda}{\sqrt{2}} - \sqrt{2} \kappa \mu_{\text{eff}}, & \lambda_{133}^{hhh} &= (c_\beta \lambda - \kappa s_\beta) v \lambda, \\ \lambda_{222}^{hhh} &= \frac{3M_Z^2 s_\beta}{v}, & \lambda_{223}^{hhh} &= \sqrt{2} \lambda \mu_{\text{eff}}, & \lambda_{233}^{hhh} &= (-c_\beta \kappa + \lambda s_\beta) v \lambda, \\ \lambda_{333}^{hhh} &= \sqrt{2} \kappa \left( \frac{6\kappa \mu_{\text{eff}}}{\lambda} + \sqrt{2} A_\kappa \right). \end{aligned} \quad (70)$$

The trilinear couplings of one CP-even Higgs boson with two CP-odd Higgs states  $a_l$  ( $l = 1, 2$ ) are obtained from the interaction eigenstates through

$$\lambda_{h_i a_l a_m} = \mathcal{R}_{i'i'}^S \mathcal{R}_{l'l'}^P \mathcal{R}_{m'm'}^P \lambda_{i'l'm'}^{haa}, \quad i, i', l', m' = 1, 2, 3, \quad l, m = 1, 2. \quad (71)$$

Here, for the indices  $i', l', m'$  we have the correspondences  $1 \hat{=} a$ ,  $2 \hat{=} a_s$ ,  $3 \hat{=} G$ . The couplings  $\lambda_{i'l'm'}^{haa}$  are symmetric with respect to an exchange of the last two indices  $l', m'$ , and

$$\begin{aligned} \lambda_{111}^{haa} &= -\frac{c_\beta c_{2\beta} M_Z^2}{v} + c_\beta^3 \lambda^2 v, & \lambda_{112}^{haa} &= c_\beta \left( \frac{A_\lambda \lambda}{\sqrt{2}} - \sqrt{2} \kappa \mu_{\text{eff}} \right), \\ \lambda_{113}^{haa} &= c_\beta^2 s_\beta \left( \frac{2M_Z^2}{v} - \lambda^2 v \right), & \lambda_{122}^{haa} &= (c_\beta \lambda + \kappa s_\beta) \lambda v, \\ \lambda_{123}^{haa} &= s_\beta \left( -\frac{A_\lambda \lambda}{\sqrt{2}} + \sqrt{2} \kappa \mu_{\text{eff}} \right), & \lambda_{133}^{haa} &= \frac{c_\beta c_{2\beta} M_Z^2}{v} + c_\beta s_\beta^2 \lambda^2 v, \\ \lambda_{211}^{haa} &= \frac{s_\beta c_{2\beta} M_Z^2}{v} + \lambda^2 s_\beta^3 v, & \lambda_{212}^{haa} &= s_\beta \left( \frac{A_\lambda \lambda}{\sqrt{2}} - \sqrt{2} \kappa \mu_{\text{eff}} \right), \\ \lambda_{213}^{haa} &= -c_\beta s_\beta^2 \left( \frac{2M_Z^2}{v} - \lambda^2 v \right), & \lambda_{222}^{haa} &= (c_\beta \kappa + s_\beta \lambda) \lambda v, \\ \lambda_{223}^{haa} &= c_\beta \left( \frac{A_\lambda \lambda}{\sqrt{2}} - \sqrt{2} \kappa \mu_{\text{eff}} \right), & \lambda_{233}^{haa} &= -\frac{c_{2\beta} s_\beta M_Z^2}{v} + c_\beta^2 s_\beta \lambda^2 v, \\ \lambda_{311}^{haa} &= s_{2\beta} \left( \frac{A_\lambda \lambda}{\sqrt{2}} + \sqrt{2} \kappa \mu_{\text{eff}} \right) + \sqrt{2} \lambda \mu_{\text{eff}}, & \lambda_{312}^{haa} &= -\kappa \lambda v, \\ \lambda_{313}^{haa} &= c_{2\beta} \left( \frac{A_\lambda \lambda}{\sqrt{2}} + \sqrt{2} \kappa \mu_{\text{eff}} \right), & \lambda_{322}^{haa} &= \frac{2\sqrt{2} \kappa^2 \mu_{\text{eff}}}{\lambda} - \sqrt{2} \kappa A_\kappa, \\ \lambda_{323}^{haa} &= 0, & \lambda_{333}^{haa} &= -s_{2\beta} \left( \frac{A_\lambda \lambda}{\sqrt{2}} + \sqrt{2} \kappa \mu_{\text{eff}} \right) + \sqrt{2} \lambda \mu_{\text{eff}}. \end{aligned} \quad (72)$$

## References

- [1] G. Aad *et al.* [ATLAS Collaboration], Phys. Lett. B **716** (2012) 1 [arXiv:1207.7214 [hep-ex]]; G. Aad *et al.* [ATLAS Collaboration], ATLAS-CONF-2012-162.
- [2] S. Chatrchyan *et al.* [CMS Collaboration], Phys. Lett. B **716** (2012) 30 [arXiv:1207.7235 [hep-ex]]; S. Chatrchyan *et al.* [CMS Collaboration], CMS-PAS-HIG-12-045.
- [3] C. Englert, T. Plehn, M. Rauch, D. Zerwas and P. M. Zerwas, Phys. Lett. B **707** (2012) 512 [arXiv:1112.3007 [hep-ph]]; J. R. Espinosa, C. Grojean, M. Muhlleitner and M. Trott, JHEP **1205** (2012) 097 [arXiv:1202.3697 [hep-ph]]; P. P. Giardino, K. Kannike, M. Raidal and A. Strumia, JHEP **1206** (2012) 117 [arXiv:1203.4254 [hep-ph]]; J. Ellis and T. You, JHEP **1206** (2012) 140 [arXiv:1204.0464 [hep-ph]]; A. Azatov, R. Contino, D. Del Re, J. Galloway, M. Grassi and S. Rahatlou, JHEP **1206** (2012) 134 [arXiv:1204.4817 [hep-ph]]; M. Klute, R. Lafaye, T. Plehn, M. Rauch and D. Zerwas, Phys. Rev. Lett. **109** (2012) 101801 [arXiv:1205.2699 [hep-ph]]; I. Low, J. Lykken and G. Shaughnessy, Phys. Rev. D **86** (2012) 093012 [arXiv:1207.1093 [hep-ph]]; T. Corbett, O. J. P. Eboli, J. Gonzalez-Fraile and M. C. Gonzalez-Garcia, Phys. Rev. D **86** (2012) 075013 [arXiv:1207.1344 [hep-ph]]; P. P. Giardino, K. Kannike, M. Raidal and A. Strumia, Phys. Lett. B **718** (2012) 469 [arXiv:1207.1347 [hep-ph]]; J. Ellis and T. You, JHEP **1209** (2012) 123 [arXiv:1207.1693 [hep-ph]]; J. R. Espinosa, C. Grojean, M. Muhlleitner and M. Trott, JHEP **1212** (2012) 045 [arXiv:1207.1717 [hep-ph]]; D. Carmi, A. Falkowski, E. Kuflik, T. Volansky and J. Zupan, JHEP **1210** (2012) 196 [arXiv:1207.1718 [hep-ph]]; F. Bonnet, T. Ota, M. Rauch and W. Winter, Phys. Rev. D **86** (2012) 093014 [arXiv:1207.4599 [hep-ph]]; T. Plehn and M. Rauch, Europhys. Lett. **100** (2012) 11002 [arXiv:1207.6108 [hep-ph]]; G. Moreau, Phys. Rev. D **87** (2013) 015027 [arXiv:1210.3977 [hep-ph]].
- [4] *See e.g.:* D. J. Miller, 2, S. Y. Choi, B. Eberle, M. M. Muhlleitner and P. M. Zerwas, Phys. Lett. B **505** (2001) 149 [hep-ph/0102023]; T. Plehn, D. L. Rainwater and D. Zeppenfeld, Phys. Rev. Lett. **88** (2002) 051801 [hep-ph/0105325]; S. Y. Choi, D. J. Miller, M. M. Muhlleitner and P. M. Zerwas, Phys. Lett. B **553** (2003) 61 [hep-ph/0210077]; K. Odagiri, JHEP **0303** (2003) 009 [hep-ph/0212215]; C. P. Buszello, I. Fleck, P. Marquard and J. J. van der Bij, Eur. Phys. J. C **32** (2004) 209 [hep-ph/0212396]; J. R. Ellis, J. S. Lee and A. Pilaftsis, Phys. Rev. D **70** (2004) 075010 [hep-ph/0404167]; S. Y. Choi, J. Kalinowski, Y. Liao and P. M. Zerwas, Eur. Phys. J. C **40** (2005) 555 [hep-ph/0407347]. C. P. Buszello and P. Marquard, hep-ph/0603209; R. M. Godbole, D. J. Miller and M. M. Muhlleitner, JHEP **0712** (2007) 031 [arXiv:0708.0458 [hep-ph]]; S. Berge, W. Bernreuther and J. Ziethe, Phys. Rev. Lett. **100** (2008) 171605 [arXiv:0801.2297 [hep-ph]]; S. Berge and W. Bernreuther, Phys. Lett. B **671** (2009) 470 [arXiv:0812.1910 [hep-ph]]; K. Hagiwara, Q. Li and K. Mawatari, JHEP **0907** (2009) 101 [arXiv:0905.4314 [hep-ph]]; Y. Gao, A. V. Gritsan, Z. Guo, K. Melnikov, M. Schulze and N. V. Tran, Phys. Rev. D **81** (2010) 075022 [arXiv:1001.3396 [hep-ph]]; A. De Rujula, J. Lykken, M. Pierini, C. Rogan and M. Spiropulu, Phys. Rev. D **82** (2010) 013003 [arXiv:1001.5300 [hep-ph]]; N. D. Christensen, T. Han and Y. Li, Phys. Lett. B **693** (2010) 28 [arXiv:1005.5393 [hep-ph]]; C. En-

- glert, C. Hackstein and M. Spannowsky, Phys. Rev. D **82** (2010) 114024 [arXiv:1010.0676 [hep-ph]]; U. De Sanctis, M. Fabbrichesi and A. Tonero, Phys. Rev. D **84** (2011) 015013 [arXiv:1103.1973 [hep-ph]]; S. Berge, W. Bernreuther, B. Niepelt and H. Spiesberger, Phys. Rev. D **84** (2011) 116003 [arXiv:1108.0670 [hep-ph]]. J. Ellis and D. S. Hwang, JHEP **1209** (2012) 071 [arXiv:1202.6660 [hep-ph]]; C. Englert, M. Spannowsky and M. Takeuchi, JHEP **1206** (2012) 108 [arXiv:1203.5788 [hep-ph]]; S. Bolognesi, Y. Gao, A. V. Gritsan, K. Melnikov, M. Schulze, N. V. Tran and A. Whitbeck, Phys. Rev. D **86** (2012) 095031 [arXiv:1208.4018 [hep-ph]]; R. Boughezal, T. J. LeCompte and F. Petriello, arXiv:1208.4311 [hep-ph]; D. Stolarski and R. Vega-Morales, Phys. Rev. D **86** (2012) 117504 [arXiv:1208.4840 [hep-ph]]; J. Ellis, D. S. Hwang, V. Sanz and T. You, JHEP **1211** (2012) 134 [arXiv:1208.6002 [hep-ph]]; A. Alves, Phys. Rev. D **86** (2012) 113010 [arXiv:1209.1037 [hep-ph]]. S. Y. Choi, M. M. Muhlleitner and P. M. Zerwas, Phys. Lett. B **718** (2013) 1031 [arXiv:1209.5268 [hep-ph]]; J. Ellis, R. Fok, D. S. Hwang, V. Sanz and T. You, arXiv:1210.5229 [hep-ph]; J. Ellis, R. Fok, D. S. Hwang, V. Sanz and T. You, arXiv:1210.5229 [hep-ph]; Y. Chen, N. Tran and R. Vega-Morales, JHEP **1301** (2013) 182 [arXiv:1211.1959 [hep-ph]]; A. Freitas and P. Schwaller, Phys. Rev. D **87** (2013) 055014 [arXiv:1211.1980 [hep-ph]]; J. Frank, M. Rauch and D. Zeppenfeld, Phys. Rev. D **87**, **055020** (2013) [arXiv:1211.3658 [hep-ph]]; C. Englert, D. Goncalves-Netto, K. Mawatari and T. Plehn, JHEP **1301** (2013) 148 [arXiv:1212.0843 [hep-ph]]; A. Djouadi, R. M. Godbole, B. Mellado and K. Mohan, arXiv:1301.4965 [hep-ph]; J. Frank, M. Rauch and D. Zeppenfeld, arXiv:1305.1883 [hep-ph]; R. Godbole, D. J. Miller, K. Mohan and C. D. White, arXiv:1306.2573 [hep-ph].
- [5] A. Djouadi, W. Kilian, M. Muhlleitner and P. M. Zerwas, Eur. Phys. J. C **10** (1999) 27 [hep-ph/9903229].
- [6] A. Djouadi, W. Kilian, M. Muhlleitner and P. M. Zerwas, Eur. Phys. J. C **10** (1999) 45 [hep-ph/9904287]; M. M. Muhlleitner, hep-ph/0008127.
- [7] U. Baur, T. Plehn and D. L. Rainwater, Phys. Rev. Lett. **89** (2002) 151801; Phys. Rev. D **67** (2003) 033003; Phys. Rev. D **68** (2003) 033001; Phys. Rev. D **69** (2004) 053004; R. Grober and M. Muhlleitner, JHEP **1106** (2011) 020 [arXiv:1012.1562 [hep-ph]]; M. J. Dolan, C. Englert and M. Spannowsky, JHEP **1210** (2012) 112 [arXiv:1206.5001 [hep-ph]]; A. Papaefstathiou, L. L. Yang and J. Zurita, Phys. Rev. D **87** (2013) 011301 [arXiv:1209.1489 [hep-ph]]; F. Goertz, A. Papaefstathiou, L. L. Yang and J. Zurita, arXiv:1301.3492 [hep-ph]; J. Grigo, J. Hoff, K. Melnikov and M. Steinhauser, arXiv:1305.7340 [hep-ph].
- [8] J. Baglio, A. Djouadi, R. Grober, M. M. Muhlleitner, J. Quevillon and M. Spira, arXiv:1212.5581 [hep-ph].
- [9] G. Cynolter, E. Lendvai and G. Pocsik, Acta Phys. Polon. B **31** (2000) 1749 [hep-ph/0003008]; T. Plehn and M. Rauch, Phys. Rev. D **72** (2005) 053008 [hep-ph/0507321]; T. Binoth, S. Karg, N. Kauer and R. Ruckl, Phys. Rev. D **74** (2006) 113008 [hep-ph/0608057].
- [10] *See e.g. with references therein:* A. Djouadi, Phys. Rept. **459** (2008) 1 [hep-ph/0503173].
- [11] P. Fayet, Nucl. Phys. B **90** (1975) 104; Phys. Lett. B **64** (1976) 159; Phys. Lett. B **69** (1977) 489 and Phys. Lett. B **84** (1979) 416; H.P. Nilles, M. Srednicki and D. Wyler, Phys. Lett.

- B **120** (1983) 346; J.M. Frere, D.R. Jones and S. Raby, Nucl. Phys. B **222** (1983) 11; J.P. Derendinger and C.A. Savoy, Nucl. Phys. B **237** (1984) 307; A.I. Veselov, M.I. Vysotsky and K.A. Ter-Martirosian, Sov. Phys. JETP **63** (1986) 489; J.R. Ellis, J.F. Gunion, H.E. Haber, L. Roszkowski and F. Zwirner, Phys. Rev. D **39** (1989) 844; M. Drees, Int. J. Mod. Phys. A **4** (1989) 3635.
- [12] U. Ellwanger, M. Rausch de Traubenberg and C.A. Savoy, Phys. Lett. B **315** (1993) 331, Z. Phys. C **67** (1995) 665 and Nucl. Phys. B **492** (1997) 307; U. Ellwanger, Phys. Lett. B **303** (1993) 271; P. Pandita, Z. Phys. C **59** (1993) 575; T. Elliott, S.F. King and P.L. White, Phys. Rev. D **49** (1994) 2435; S.F. King and P.L. White, Phys. Rev. D **52** (1995) 4183; F. Franke and H. Fraas, Int. J. Mod. Phys. A **12** (1997) 479.
- [13] D. J. Miller, R. Nevzorov and P. M. Zerwas, Nucl. Phys. B **681** (2004) 3 [hep-ph/0304049]; *for reviews, see:* M. Maniatis, Int. J. Mod. Phys. **A25** (2010) 3505 [arXiv:0906.0777 [hep-ph]]; U. Ellwanger, C. Hugonie, A. M. Teixeira, Phys. Rept. **496** (2010) 1 [arXiv:0910.1785 [hep-ph]]; U. Ellwanger, Eur. Phys. J. C **71** (2011) 1782 [arXiv:1108.0157 [hep-ph]].
- [14] K. Ender, T. Graf, M. Muhlleitner and H. Rzehak, Phys. Rev. D **85** (2012) 075024 [arXiv:1111.4952 [hep-ph]].
- [15] T. Graf, R. Grober, M. Muhlleitner, H. Rzehak and K. Walz, JHEP **1210** (2012) 122 [arXiv:1206.6806 [hep-ph]].
- [16] J.E. Kim and H.P. Nilles, Phys. Lett. B **138** (1984) 150.
- [17] M. Bastero-Gil, C. Hugonie, S. F. King, D. P. Roy and S. Vempati, Phys. Lett. B **489**, 359 (2000) [hep-ph/0006198]; A. Delgado, C. Kolda, J. P. Olson and A. de la Puente, Phys. Rev. Lett. **105**, 091802 (2010) [arXiv:1005.1282 [hep-ph]]; U. Ellwanger, G. Espitalier-Noel and C. Hugonie, JHEP **1109** (2011) 105 [arXiv:1107.2472 [hep-ph]]; G. G. Ross and K. Schmidt-Hoberg, arXiv:1108.1284 [hep-ph].
- [18] U. Ellwanger, Phys. Lett. **B303** (1993) 271 [hep-ph/9302224]; T. Elliott, S. F. King, P. L. White, Phys. Lett. **B305** (1993) 71 [hep-ph/9302202], Phys. Lett. **B314** (1993) 56 [hep-ph/9305282], Phys. Rev. **D49** (1994) 2435 [hep-ph/9308309]; P. N. Pandita, Z. Phys. **C59** (1993) 575, Phys. Lett. **B318** (1993) 338.
- [19] U. Ellwanger, C. Hugonie, Phys. Lett. **B623** (2005) 93 [hep-ph/0504269].
- [20] G. Degrandi and P. Slavich, Nucl. Phys. B **825** (2010) 119 [arXiv:0907.4682 [hep-ph]].
- [21] F. Staub, W. Porod, B. Herrmann, JHEP **1010** (2010) 040 [arXiv:1007.4049 [hep-ph]].
- [22] S. W. Ham, J. Kim, S. K. Oh and D. Son, Phys. Rev. D **64** (2001) 035007 [hep-ph/0104144]; S. W. Ham, S. H. Kim, S. K. OH and D. Son, Phys. Rev. D **76** (2007) 115013 [arXiv:0708.2755 [hep-ph]].
- [23] S. W. Ham, S. K. Oh and D. Son, Phys. Rev. D **65** (2002) 075004 [hep-ph/0110052]; S. W. Ham, Y. S. Jeong and S. K. Oh, hep-ph/0308264.

- [24] K. Funakubo and S. Tao, Prog. Theor. Phys. **113** (2005) 821 [hep-ph/0409294].
- [25] K. Cheung, T. -J. Hou, J. S. Lee and E. Senaha, Phys. Rev. D **82** (2010) 075007 [arXiv:1006.1458 [hep-ph]].
- [26] A. Denner, Fortsch. Phys. **41** (1993) 307 [arXiv:0709.1075 [hep-ph]].
- [27] K. Melnikov and T. v. Ritbergen, Phys. Lett. B **482** (2000) 99 [hep-ph/9912391].
- [28] M. S. Carena, D. Garcia, U. Nierste and C. E. M. Wagner, Nucl. Phys. B **577** (2000) 88 [hep-ph/9912516].
- [29] L. V. Avdeev and M. Y. Kalmykov, Nucl. Phys. B **502** (1997) 419 [hep-ph/9701308].
- [30] D. M. Pierce, J. A. Bagger, K. T. Matchev and R. -j. Zhang, Nucl. Phys. B **491** (1997) 3 [hep-ph/9606211].
- [31] M. S. Carena, J. R. Ellis, S. Mrenna, A. Pilaftsis and C. E. M. Wagner, Nucl. Phys. B **659** (2003) 145 [hep-ph/0211467].
- [32] J. Guasch, P. Haffiger and M. Spira, Phys. Rev. D **68** (2003) 115001 [hep-ph/0305101]; D. Noth and M. Spira, Phys. Rev. Lett. **101** (2008) 181801 [arXiv:0808.0087 [hep-ph]]; D. Noth and M. Spira, JHEP **1106** (2011) 084 [arXiv:1001.1935 [hep-ph]]; L. Mihaila and C. Reisser, JHEP **1008** (2010) 021 [arXiv:1007.0693 [hep-ph]].
- [33] A. Dabelstein, Nucl. Phys. B **456** (1995) 25 [hep-ph/9503443].
- [34] M. Frank, T. Hahn, S. Heinemeyer, W. Hollik, H. Rzehak, and G. Weiglein, JHEP **0702** (2007) 047 [hep-ph/0611326].
- [35] K. E. Williams and G. Weiglein, Phys. Lett. B **660** (2008) 217 [arXiv:0710.5320 [hep-ph]].
- [36] N. Baro, F. Boudjema and A. Semenov, Phys. Rev. D **78** (2008) 115003 [arXiv:0807.4668 [hep-ph]].
- [37] K. E. Williams, H. Rzehak and G. Weiglein, Eur. Phys. J. C **71** (2011) 1669 [arXiv:1103.1335 [hep-ph]].
- [38] F. Staub, [arXiv:0806.0538 [hep-ph]], Comput. Phys. Commun. **181** (2010) 1077 [arXiv:0909.2863 [hep-ph]], Comput. Phys. Commun. **182** (2011) 808 [arXiv:1002.0840 [hep-ph]].
- [39] J. Kublbeck, M. Bohm and A. Denner, Comput. Phys. Commun. **60** (1990) 165; T. Hahn, Comput. Phys. Commun. **140** (2001) 418 [hep-ph/0012260].
- [40] T. Hahn and M. Perez-Victoria, Comput. Phys. Commun. **118** (1999) 153 [hep-ph/9807565]; T. Hahn, Comput. Phys. Commun. **178** (2008) 217 [hep-ph/0611273].
- [41] J. Beringer *et al.* [Particle Data Group Collaboration], Phys. Rev. D **86** (2012) 010001.
- [42] F. Jegerlehner, Nuovo Cim. C **034S1** (2011) 31 [arXiv:1107.4683 [hep-ph]].

- [43] The ATLAS Collaboration, ATLAS-CONF-2013-047 and ATLAS-CONF-2012-104; The CMS Collaboration, arXiv:1212.6961 [hep-ex] and arXiv:1303.2985 [hep-ex].
- [44] The ATLAS Collaboration, ATLAS-CONF-2013-024; ATLAS-CONF-2013-025, ATLAS-CONF-2013-037; ATLAS-CONF-2013-048, ATLAS-CONF-2013-053; Eur. Phys. J. C **72** (2012) 2237 [arXiv:1208.4305 [hep-ex]]; Phys. Lett. B **720** (2013) 13 [arXiv:1209.2102 [hep-ex]]; The CMS Collaboration, CMS-PAS-SUS-13-011; arXiv:1212.6961 [hep-ex]; JHEP **1301** (2013) 077; CMS-PAS-SUS-11-030.
- [45] S. F. King, M. Muhlleitner and R. Nevzorov, Nucl. Phys. B **860** (2012) 207 [arXiv:1201.2671 [hep-ph]].
- [46] S. F. King, M. Muhlleitner, R. Nevzorov and K. Walz, Nucl. Phys. B **870** (2013) 323 [arXiv:1211.5074 [hep-ph]].
- [47] The ATLAS Collaboration, JHEP **1206** (2012) 039 [arXiv:1204.2760 [hep-ex]]; ATLAS-CONF-2012-011 and ATLAS-CONF-2011-094; The CMS Collaboration, JHEP **1207** (2012) 143 [arXiv:1205.5736 [hep-ex]].
- [48] The ATLAS Collaboration, ATLAS-CONF-2013-034.
- [49] The CMS Collaboration, CMS-PAS-HIG-13-005.
- [50] A. Djouadi, J. Kalinowski and M. Spira, Comput. Phys. Commun. **108**, 56 (1998) [hep-ph/9704448].
- [51] A. Djouadi, M. M. Muhlleitner and M. Spira, Acta Phys. Polon. B **38** (2007) 635 [hep-ph/0609292].
- [52] U. Ellwanger, J.F. Gunion and C. Hugonie, JHEP **0502** (2005) 066; U. Ellwanger and C. Hugonie, Comput. Phys. Commun. **175** (2006) 290.
- [53] U. Ellwanger and C. Hugonie, Comput. Phys. Commun. **177** (2007) 399; (see also <http://www.th.u-psud.fr/NMHDECAY/nmssmtools.html>).
- [54] M. Muhlleitner, A. Djouadi and Y. Mambrini, Comput. Phys. Commun. **168** (2005) 46 [hep-ph/0311167]; M. Muhlleitner, Acta Phys. Polon. B **35** (2004) 2753 [hep-ph/0409200].
- [55] P. Bechtle, O. Brein, S. Heinemeyer, G. Weiglein and K. E. Williams, Comput. Phys. Commun. **181** (2010) 138 [arXiv:0811.4169 [hep-ph]]; P. Bechtle, O. Brein, S. Heinemeyer, G. Weiglein and K. E. Williams, Comput. Phys. Commun. **182** (2011) 2605 [arXiv:1102.1898 [hep-ph]]; *see also references therein.*
- [56] The ATLAS Collaboration, ATLAS-CONF-2013-012 and ATLAS-CONF-2012-168; The CMS Collaboration, CMS-PAS-HIG-13-001.
- [57] The ATLAS Collaboration, ATLAS-CONF-2013-013; The CMS Collaboration, CMS-PAS-HIG-13-002.
- [58] The ATLAS Collaboration, ATLAS-CONF-2013-030.



- [59] S. Kanemura, Y. Okada, E. Senaha and C. -P. Yuan, Phys. Rev. D **70** (2004) 115002 [hep-ph/0408364].
- [60] W. Hollik and S. Penaranda, Eur. Phys. J. C **23** (2002) 163 [hep-ph/0108245].
- [61] A. Dobado, M. J. Herrero, W. Hollik and S. Penaranda, Phys. Rev. D **66** (2002) 095016 [hep-ph/0208014].
- [62] S. Kanemura, T. Shindou and K. Yagyu, Phys. Lett. B **699** (2011) 258 [arXiv:1009.1836 [hep-ph]].
- [63] E. W. N. Glover and J. J. van der Bij, Nucl. Phys. B **309** (1988) 282.
- [64] T. Plehn, M. Spira and P. M. Zerwas, Nucl. Phys. B **479** (1996) 46 [Erratum-ibid. B **531** (1998) 655] [hep-ph/9603205].
- [65] S. Dawson, S. Dittmaier and M. Spira, Phys. Rev. D **58** (1998) 115012 [hep-ph/9805244].
- [66] W. Y. Keung, Mod. Phys. Lett. A2 (1987) 765; D. Dicus, K. Kallianpur and S. Willenbrock, Phys. Lett. B200 (1988) 187; K. Kallianpur, Phys. Lett. B215 (1988) 392; A. Abbasabadi, W.W. Repko, D.A. Dicus and R. Vega, Phys. Rev. **D38** (1988) 2770; Phys. Lett. B213 (1988) 386; A. Dobrovolskaya and V. Novikov, Z. Phys. C52 (1991) 427.
- [67] V. Barger, T. Han and R.J.N. Phillips, Phys. Rev. **D38** (1988) 2766.
- [68] M. Moretti, S. Moretti, F. Piccinini, R. Pittau and A. D. Polosa, JHEP **0502** (2005) 024 [hep-ph/0410334].
- [69] URL: <http://people.web.psi.ch/spira/hpair/>
- [70] M. Gillioz, R. Grober, C. Grojean, M. Muhlleitner and E. Salvioni, JHEP **1210** (2012) 004 [arXiv:1206.7120 [hep-ph]].
- [71] M. Spira, hep-ph/9510347.
- [72] D. Graudenz, M. Spira and P. M. Zerwas, Phys. Rev. Lett. **70** (1993) 1372; M. Spira, A. Djouadi, D. Graudenz and P. M. Zerwas, Phys. Lett. B **318** (1993) 347; M. Spira, A. Djouadi, D. Graudenz and P. M. Zerwas, Nucl. Phys. B **453** (1995) 17 [hep-ph/9504378].
- [73] S. Dawson, A. Djouadi and M. Spira, Phys. Rev. Lett. **77** (1996) 16 [hep-ph/9603423].
- [74] M. Muhlleitner and M. Spira, Nucl. Phys. B **790** (2008) 1 [hep-ph/0612254].
- [75] S. Dittmaier *et al.* [LHC Higgs Cross Section Working Group Collaboration], arXiv:1101.0593 [hep-ph].
- [76] A. D. Martin, W. J. Stirling, R. S. Thorne and G. Watt, Eur. Phys. J. C **63** (2009) 189 [arXiv:0901.0002 [hep-ph]].